UTRECHT UNIVERSITY

Institute for Marine and Atmospheric Research Utrecht (IMAU)

Climate Physics master thesis

Climate response of abrupt and steady stratospheric aerosol injection

By:

Fiona Román de Miguel

Student number: 8075034

Supervisors:

Claudia Wieners, Daniel Pflüger, Michiel Baatsen

July 4, 2023

Abstract

As the consequences of climate change become more evident, efforts are being made to find ways to mitigate these effects. A promising temporary solution is Stratospheric Aerosol Injection (SAI), which is based on reflecting part of the incoming radiation back to space to lower the Earth temperature. Using the Community Earth System Model version 2 (CESM2) with the Community Atmosphere Model version 6 (CAM6) as its atmospheric component, three simulations were made: a high emission scenario called CONTROL, a scenario where SAI is deployed in 2020 (SAI 2020) and a high emission scenario until 2080, when SAI is implemented (SAI 2080). In this project we analyse these simulations to know what effect does it have on temperature, precipitation and precipitation minus evaporation to start SAI in 2020 or to wait until 2080. We find that, although Greenland overcools in SAI 2080, temperature and precipitation globally decrease under both geoengineering simulations relative to CONTROL. Additionally, SAI also keeps values close to present-day conditions, meaning that the geoengineering simulations can partially restore the climate. However, we prove that waiting until 2080 to implement SAI can have negative effects for some ecosystems. Finally, we acknowledge that future research should be made continuing this path.

Contents

1 Introduction

Global warming is undeniably a part of humanity's present and future. While efforts have been made to combat rising temperatures, the efficacy of these measures is still uncertain, and the possibility remains that they may fall short of what is required. As a result, a new concept has grown within the scientific community during these past years, the so-called geoengineering. Geoengineering comprises two distinct components aimed at mitigating global warming: carbon removal and solar geoengineering. Carbon removal seeks to extract carbon dioxide from the atmosphere to limit its heat-trapping capacity, while solar geoengineering aims to reflect more sunlight away from the planet to reduce heat absorption. This project focuses on a specific type of solar geoengineering, called stratospheric aerosol injection.

Stratospheric aerosol injection (from now on, SAI) represents a promising yet also controversial temporary solution to global warming. It works by introducing aerosols into the stratosphere to create a thin layer that reflects the sunlight back to outer space, causing temperatures to drop (Crutzen, 2006). SAI aims to imitate what naturally happens when there is a big volcanic eruption, such as the Mount Pinatubo eruption in 1991. This volcanic event released about 17 Tg of sulphur dioxide into the middle to lower stratosphere, resulting in a notable cooling of the Northern Hemisphere (NH) of around 0.5ºC during 1992-1993 (Self et al., 1993).

First, we will present the advantages of this solar geoengineering method, and then we will consider the disadvantages. The advantages of SAI are that it is a cheap method to deploy in comparison to other geoengineering techniques (Smith and Wagner, 2018; Tracy et al., 2022), and that there is high agreement that it can work to achieve the temperature target established in Paris 2015 [1] (Irvine et al., 2019; Tilmes et al., 2020; Pamplany et al., 2020; de Coninck et al., 2020; Tracy et al., 2022). Also, SAI could potentially support mitigation efforts by promoting awareness regarding climate change (Pamplany et al., 2020).

[1] Paris Agreement 2015: international treaty on climate change. Its goal is to limit the increase in the global average temperature below 2ºC above pre-industrial (PI) levels and pursue efforts to limit the temperature increase to 1.5ºC above PI.

However, the disadvantages of SAI are that it is believed that precipitation will be reduced if SAI is implented (Irvine et al., 2019; Tilmes et al., 2020) and that given the lack of previous studies on the field, there are still many uncertainties and side effects (MacMartin and Kravitz, 2019; Pamplany et al., 2020). In addition, the moral implications of SAI make it a controversial topic. One argument against it is the "playing God" argument, which holds that humans lack the authority to artificially alter something as vast as the atmosphere (Robock et al., 2009; Hulme, 2012). Another argument is that SAI, if ever deployed, would have an unequal representation as it would be controlled by wealthy countries (i.e., NH countries) (de Coninck et al., 2020; Pamplany et al., 2020). However, there is scientific evidence that the bad consequences would impact the poorer countries, which are typically in the Southern Hemisphere (SH); is SAI then a solution only for the rich? (Biernmann and Möller, 2019).

This project is different from previous work because it studies the different effects on the climate if SAI is initiated in 2020 versus in 2080. The underlying idea for waiting until 2080 to implement SAI is based on a hypothetical scenario where humanity fails to take significant action against climate change and, eventually, people realize the urgent need to cool down the Earth, leading to the deployment of SAI. Moreover, given the limited knowledge surrounding SAI, delaying deployment until 2080 represents a feasible approach. Changing the starting date does not have a notable effect on the final achievement (which is to lower the mean surface temperature), but on the way to achieve it. Therefore, the main research question is how important meteorological variables, such as temperature or precipitation, will change depending on the geoengineering scenario. Another question we tried to answer within this project is if SAI restores the climate, i.e., if it brings the future climate close to the conditions that were at a certain moment in the past. From this second question another one arises: even if SAI is deployed in 2080, can it still restore the climate? Additionally, we analysed variables that have significant impacts on ecological systems. By exploring these parameters, we seek to understand the ecological implications of SAI deployment.

Section 2 describes the model, the simulations used in this project and the methodology followed to analyze the data. The outcome of this analysis is presented in Section 3. Discussions and conclusions are presented in Sections 4 and 5, respectively.

2 Methodology

2.1 Model

The simulations used in this study were made with the Community Earth System Model version 2 (CESM2), which operates at 1° horizontal resolution and gives global data. CESM2 encompasses various models that exchange states via a coupler, each of those models responsible for simulating different aspects of the Earth system. These models are CAM6 for the atmospheric component, CICE for the sea-ice, CLM for the land, MOSART for the river, POP2 for the ocean, CSIM for the land-ice, and WW3 for the ocean-wave component. Specifics regarding the configuration of CESM2, along with an overview of its performance, can be found in Danabasoglu et al., 2020.

The analysed data in this work comes only from the atmospheric model CAM6 (Community Atmosphere Model version 6), which was used with the same resolution as CESM2.

2.2 Simulations and Data

The simulations used in this project aim to replicate the two simulations conducted by Tilmes et al., 2018. The first one, denoted as CONTROL, represents a high emission scenario characterized by the Representative Concentration Pathway 8.5 (RCP8.5). The second simulation (SAI 2020) incorporates SAI from the year 2020 with the aim of limiting global mean surface temperature (GMST) increase to within 1.5ºC above pre-industrial (PI) levels. Additionally, a third simulation was performed wherein the RCP8.5 pathway was followed until 2080, when SAI was suddenly implemented to induce a rapid reduction of temperatures back to PI levels. A detailed explanation of the CONTROL and the SAI 2020 simulations can be found in Tilmes et al., 2018, and an overview of the three simulations is presented in Table 1.

Name	Description	Frequency	Time span
Control	High emission scenario	Daily and monthly data	2015-2100
SAI 2020	Deploys SAI in 2020 to keep GMST below 1.5ºC above PI	Daily and monthly data	2020-2100 (monthly), 2090-2100 (daily)
SAI 2080	High emission scenario until 2080, when SAI is abruptly deployed	Daily and monthly data	2080-2100

Table 1: General information about the simulations used in this project.

Several experiments have been made within the Geoengineering Model Intercomparison Project (GeoMIP) to try to simulate SAI in climate models. GeoMIP was intially suggested in Kravitz et al., 2011, with the idea of establishing a standardized framework for conducting solar radiation management (SRM) [2] modelling experiments. By doing so, it was possible not only to better compare the different model responses, but also to determine the main sources of uncertainties.

There are distinct approaches for simulating a non-warming Earth, all of them included in GeoMIP. The first one involves reducing the total solar irradiance, effectively counterbalancing the temperature rise caused by increased greenhouse gas levels. This reduction can be achieved by decreasing the solar constant (Kravitz et al., 2021). However, it is important to note that this approach, while computationally straightforward, lacks a physical basis. The second approach provides a more realistic representation but is computationally intense, and it consists of injecting a constant amount of SO_2 into the equatorial stratosphere (Tilmes et al., 2018). To alleviate computational burdens, there is a third way in which it is possible to model a non-warming Earth. This third approach takes the output of the simulation conducted with the chemical model and adjusts it by changing the simulated stratospheric aerosol optical depth (AOD) (Kravitz et al., 2021).

[2] SRM: type of solar geoengineering that refers to deliberate modification of the Earth's climate system to reduce the amount of solar radiation that reaches the planet's surface. It includes SAI.

Since CAM6 does not model aerosol dynamics, this third approach is the one used to produce our data. The aerosol fields derived from the Whole Atmosphere Community Climate Model (WACCM) simulations were used as an external forcing, and their intensity was reconstructed adjusting the AOD. Therefore, the stratospheric aerosols concentration was prescribed using an algorithm that ensured that GMST kept its target.

In order to facilitate a more comprehensive analysis of the data, it was necessary to establish a reference period (REF) so the output could be compared with. Ideally, the reference period would have been the PI conditions, but that was not possible as the earliest simulation only starts in 2015. Consequently, we defined the reference period as the average between 2015 and 2030 from the CONTROL simulation. It is important to remark that this reference time span already includes some anthropogenic warming.

For the analysis, the data was divided into 15-year intervals. Although the conventional practice is to consider a 30-year period for climate data analysis, we deviated from this norm due to the time span of the SAI 2080 simulation. The first 5 to 10 years of SAI 2080 represent a very transitional phase, as the climate system is still adjusting to the new conditions, so a 20-year interval would not have been optimal. As a compromise, we selected a 15-year interval to ensure a higher representation of characteristic years and facilitate a more accurate analysis.
As we were only interested in the changes over land, we included a land mask in all our analysis, so the ocean was ignored and only the land was studied.

The variables examined in this study are the reference height temperature (TREFHT), the total precipitation (PRECT), the maximum 5-day precipitation (max5) and the total precipitation minus evaporation (PE). Some observations regarding the variables:

- Reference height temperature: also known as near-surface air temperature, is calculated by interpolating the surface temperature and the lowest model level temperature.
- Total precipitation: encompasses both convective and large-scale precipitation components, with the former playing a significant role in influencing its overall magnitude.

- Maximum 5-day precipitation: represents the average of the annual maximum 5-day precipitation over a period of 10 years. In this case, the mean was based on a shorter time frame of 10 years instead of 15 given that the daily mean data for the SAI 2020 simulation only goes from 2090 to 2100. Given the limited time span, it is important to acknowledge that the max5 analysis holds a lower degree of reliability.
- Precipitation minus evaporation: as evaporation is not directly obtained as an output of the simulations, it was calculated as:

$$evaporation = \frac{latent\ heat\ flux}{latent\ heat\ of\ evaporation\ of\ water} \tag{1}$$

2.3 Background information

2.3.1 Regional analysis

To analyse the data regionally we used the Intergovernmental Panel on Climate Change (IPCC) Special Report on Extremes (SREX) region definition ("AR5 Reference Regions", n.d.). These definitions were used to create masks that were later applied to the data. The above-mentioned IPCC SREX regions represent areas of significant climatic coherence, and quickly emerged as the preferred framework for conducting regional analysis in various applications (Iturbide et al., 2020).

As our project exclusively focuses on land, certain regions encompassing oceanic areas were not taken into account when performing the analysis. These excluded regions are distinguished by a star symbol next to their short names in Figure 1.

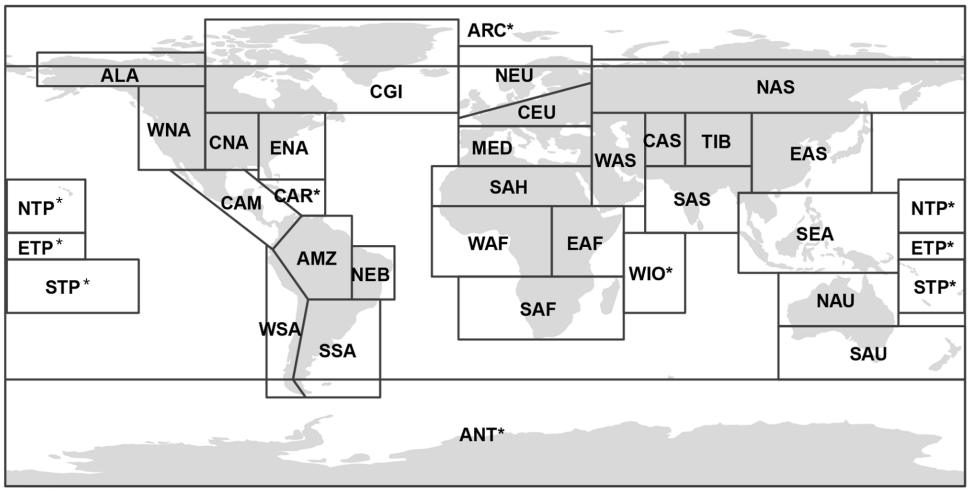

Figure 1: IPCC SREX reference regions. The full name of every region is written in Table 2. The regions with a star symbol have been excluded from our analysis. Source: Iturbide et al., 2020.

ALA: Alaska / North West Canada	CNA: Central North America	NAU: North Australia	SAU: South Australia / New Zealand	WNA: West North America
AMZ: Amazon	EAF: East Africa	NEB: North East Brazil	SEA: South East Asia	WSA: West Coast South America
CAM: Central America / Mexico	EAS: East Asia	NEU: North Europe	SSA: South East South America	
CAS: Central Asia	ENA: East North America	SAF: South Africa	TIB: Tibetan Plateau	
CEU: Central Europe	MED: South Europe / Mediter-ranean	SAH: Sahara	WAF: West Africa	
CGI: Canada / Greenland / Iceland	NAS: North Asia	SAS: South Asia	WAS: West Asia	

Table 2: Full name of the IPCC SREX reference regions.

2.3.2 Köppen climate classification

The Köppen climate classification system is a method for categorizing climates based on the annual cycle of monthly air temperature and precipitation. Originally introduced by Köppen in 1900, it has undergone several modifications. The Köppen-Geiger classification (KGC) (Peel et al., 2007) in 1936 and the Köppen-Trewartha classification (KTC) (Feng et al., 2011) in 1954 are the two most important developments, with our project employoing the KGC.

Climate exerts a direct influence not only on global ecosystems and the distribution of

plants and animals species, but also on the economic and social systems. Its impacts extend to factors such as changes in the supply of food and water, as well as in goods and services (Cui et al., 2021). Given the changes induced by climate change in the spatial distribution of flora and fauna, it is important to quantify the impacts of the current environmental crisis on the Earth's terrestrial ecosystems. The Köppen climate classification provides a valuable method to represent shifts in climatic conditions, giving an ecologically relevant characterization of regional climate (Lohmann et al., 1993).

As previously indicated, the Köppen climate scheme divides the climate into five main groups, distinguishing various vegetation groups (Feng et al., 2011): A (Tropical), B (Dry), C (Temperate), D (Continental) and E (Polar). Within these groups, further divisions are made based on the seasonal precipitation (2nd classification) and on temperature (3rd classification), leading to a comprehensive classification (Table 3). Note how not all the groups have the three types of classification.

1st	2nd	3rd
A (Tropical)	f (Rainforest) m (Monsoon) w (Savanna, dry winter) s (Savanna, dry summer)	
B (Dry)	W (Arid desert) S (Semi arid or steppe)	h (Hot) k (Cold)
C (Temperate)	w (Dry winter) f (No dry season) s (Dry summer)	a (Hot summer) b (Warm summer) c (Cold summer)
D (Continental)	w (Dry winter) f (No dry season) s (Dry summer)	a (Hot summer) b (Warm summer) c (Cold summer) d (Very cold summer)
E (Polar)		T (Tundra) F (ice cap)

Table 3: Köppen climate classification. The first letter indicates the main group, the second one the seasonal precipitation, and the third one the level of heat.

The table above was created based on the following criteria (Peel et al., 2007):

Group A: tropical climates

Each month of the year has a mean temperature of 18ºC or higher. The subcategories within this group are as follows:

- Af (tropical rainforest): the mean precipitation throughout the year exceeds or equals 60 mm.
- Am (tropical monsoon): the driest month of the year has a mean precipitation

lower than 60 mm, but higher than a threshold calculated using the formula:

$$100 - \left(\frac{\text{total annual prec. [mm]}}{25}\right) \tag{2}$$

- Aw/As (tropical savanna): similar to the tropical monsoon, the driest month's mean precipitation is smaller than the threshold mentioned above.

Group B: Dry climates

The precipitation threshold is determined by multiplying the annual mean temperature in ºC by 20, and then adding a specific value based on the precipitation distribution during spring and summer (from April to September in the NH, or from October to March in the Southern):

- If at least 70% of the total precipitation is received during spring and summer, an additional 280 is added.
- If the total precipitation received during spring and summer ranges from 30% to 70%, an additional 140 is added.
- If less than 30% of the total precipitation is received during spring and summer, no additional value is added.

If the annual precipitation is less than 50% of this threshold, the climate is classified as BW (arid desert); if it is higher, the climate is BS (semi-arid steppe).
Lastly, the temperature classification within this group is determined by the mean temperature during the coldest month:

- h (hot): the mean temperature in the coldest month is greater than 0ºC.
- k (cold): the mean temperature in the coldest month is lower than 0ºC.

Therefore, the four possible groups are BWh (hot desert), BWk (cold desert), BSh (hot semi-arid) and BSk (cold semi-arid).

Group C: temperate climates

The coldest month of the year has a mean temperature between 0ºC and 18ºC.
The classification criteria for precipitation and temperature are as follows:

- Precipitation conditions:
  - w: precipitation in the wettest summer month is higher than 10 times the

precipitation in the driest winter month.

  - s: precipitation in the wettest winter month is at least 3 times bigger than in the driest summer month.
  - f: otherwise

- Temperature conditions:
  - a: the warmest month has a mean temperature greater than 22ºC.
  - b: all months have an average temperature lower than 22ºC and at least 4 months have a mean temperature higher than 10ºC.
  - c: only 1 to 3 months have a mean temperature higher than 10ºC.

The possible climates within this group are: Cfa (humid subtropical), Cfb (oceanic), Cfc (subpolar oceanic), Cwa (monsoon-influenced humid subtropical), Cwb (subtropical highland), Cwc (cold subtropical highland), Csa (hot-summer mediterranean), Csb (warm-summer mediterranean) and Csc (cold-summer mediterranean).

Group D: continental climates

The coldest month of the year has a mean temperature lower than 0ºC and the warmest a mean temperature bigger than 10ºC.

The precipitation and temperature conditions are the same than in group C, with the addition of an extra temperature category denoted as *d*. This category applies to regions with a mean temperature lower than -38ºC during their coldest month of the year (i.e., a point is in *d* if, in addition to the precipitation conditions for group C, its coldest month is below -38ºC).

The possible climates within group D include:

- Dfa (hot-summer humid)
- Dfb (warm-summer humid)
- Dfc (subarctic climate)
- Dfd (extremely cold subarctic)
- Dwa (monsoon-influenced hot-summer humid)
- Dwb (monsoon-influenced warm-summer humid)
- Dwc (monsoon-influenced subarctic)

- Dwd (monsoon-influenced extremely cold subarctic)
- Dsa (mediterranean-influenced hot-summer humid)
- Dsb (mediterranean-influenced warm-summer humid)
- Dsc (mediterranean-influenced subarctic)
- Dsd (mediterranean-influenced extremely cold subarctic)

Group E: polar climates

Every month of the year maintains a mean temperature smaller than 10ºC. The two possible subcategories are:

- ET (tundra): the warmest month has a mean temperature ranging between 0ºC and 10ºC.
- EF (ice cap): every month has a negative mean temperature.

Despite its good performance, the Köppen classification has various limitations (Cui et al., 2021), mainly:

1. Inflexibility in accounting for the appearance of new climate types.
2. Lack of a quantitative measure to assess the similarities and differences between local climates, as it relies on a threshold-based categorization.
3. Significant uncertainties in establishing a connection between climate zones and actual biome [3] distributions.

[3] Biome: large-scale ecological community characterized by distinct climate, vegetation and animal species. For example: tropical rainforests, deserts, tundras, etc.

3 Results

3.1 Climate analysis

3.1.1 General changes

To get a general sense of how the simulations worked we made global maps for every studied variable. We plotted the last 15 years of every simulation (so from 2085 until 2100) with respect to the reference period. To better visualize the changes SAI can make, we also included the difference between the last 15 years of SAI 2080 with respect to the CONTROL 2065-2080 average (bottom-right panel of every figure). The plots are shown in Figures 2, 3, 4 and 5.

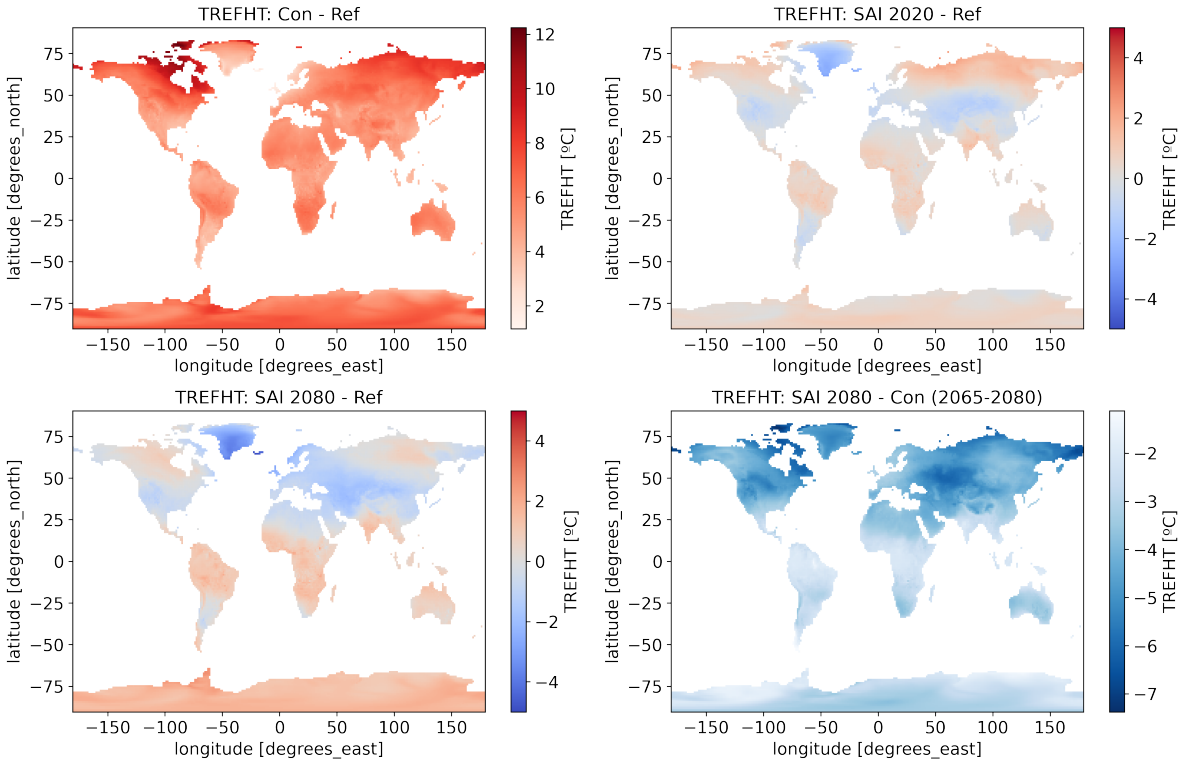

Figure 2: Difference between the 2085-2100 average of every simulation and the reference period (top and bottom-left plots), and between SAI 2080 (2085-2100) and CONTROL (2065-2080) (bottom-right plot) for the reference height temperature.

Looking at Figure 2 one can make several observations. Firstly, the plotted difference is smaller in the geoengineering simulations than in CONTROL, aligning with expectations that the high emission scenario would warm more than the geoengineering alternatives. Secondly, we see how there are some areas where SAI is able to reduce

the temperature, like Greenland and the region between 30ºN-40ºN in Asia. To better see this cooling effect, we can look at the bottom-right plot, which shows how SAI 2080 effectively cools down globally, with a bigger decrease in the North Pole. Finally, we observe how across all three scenarios, Greenland appears to experience the least warming, even cooling for SAI 2020 and SAI 2080. Looking at the scale, we observe how in the late geoengineering case, Greenland experiences the most cooling (see Section 4.3).

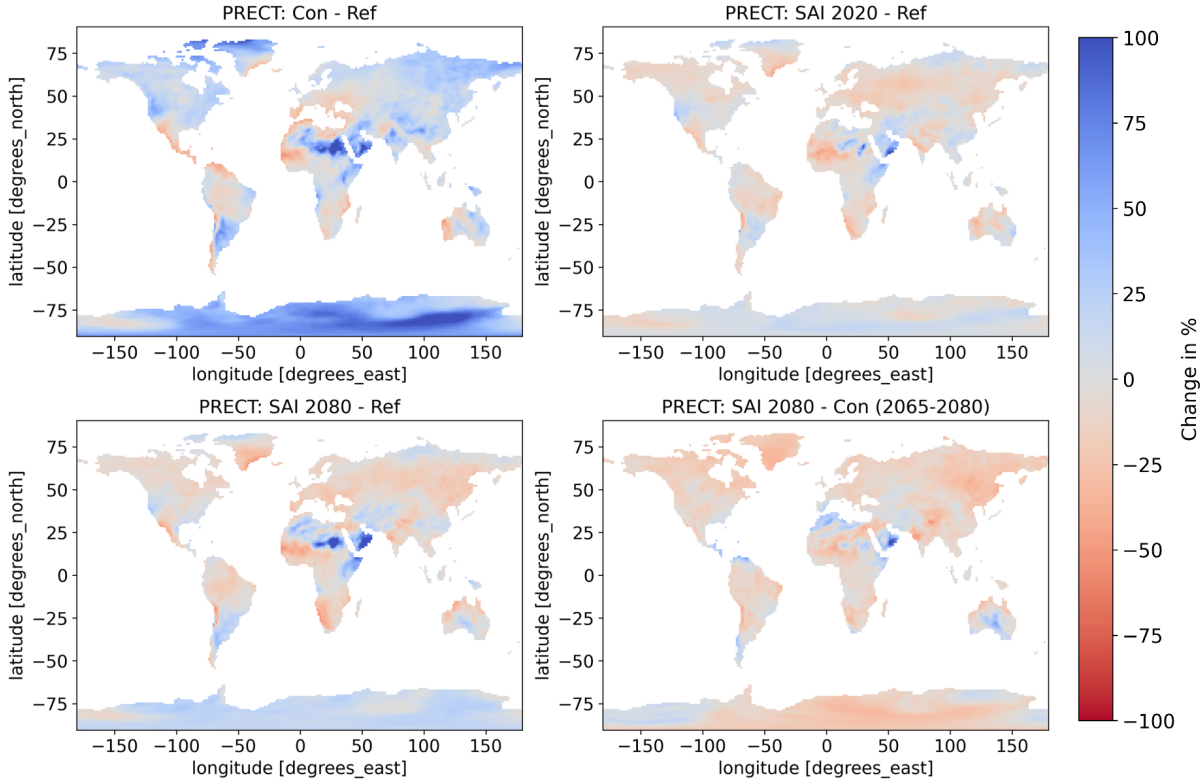

Figure 3: Difference between the 2085-2100 average of every simulation and the reference period (top and bottom-left plots), and between SAI 2080 (2085-2100) and CONTROL (2065-2080) (bottom-right plot) for the total precipitation. The change is shown in percentage.

The difference in Figures 3 and 4 is expressed in percentage for a better understanding of the relative impact of the change. One can observe that in general, in the CONTROL simulation precipitation increases while in the SAI scenarios decreases, with the notable exception of the Arabic peninsula and Antarctica. The bottom-right plots of both figures show this decrease in rainfall more clearly, as the presence of red colors indicates that the amount of rain is higher in CONTROL than in SAI 2080. It is worth noting how precipitation over Antarctica increases in all the cases, especially in the CONTROL simulation. This increase is the result of warmer temperatures, which lead to higher evaporation, resulting in more rain.

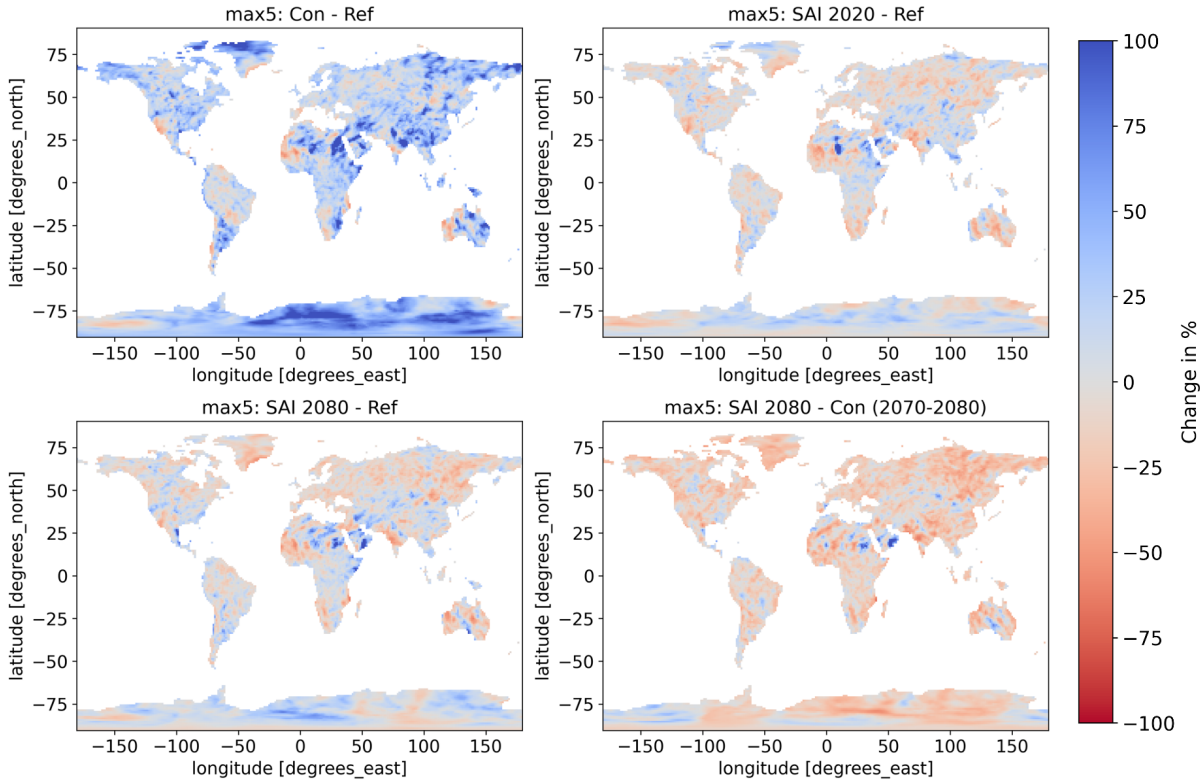

Figure 4: Difference between the 2085-2100 average of every simulation and the reference period (top and bottom-left plots), and between SAI 2080 (2085-2100) and CONTROL (2065-2080) (bottom-right plot) for the maximum 5-day precipitation. The change is shown in percentage.

Finally, Figure 5 seems to imply a level of independence between the changes in precipitation minus evaporation and the scenarios, as all three simulations present similar patterns. Regions displaying negative PE values indicate a decrease in precipitation, an increase in temperature leading to enhanced evaporation, or a combination of both.

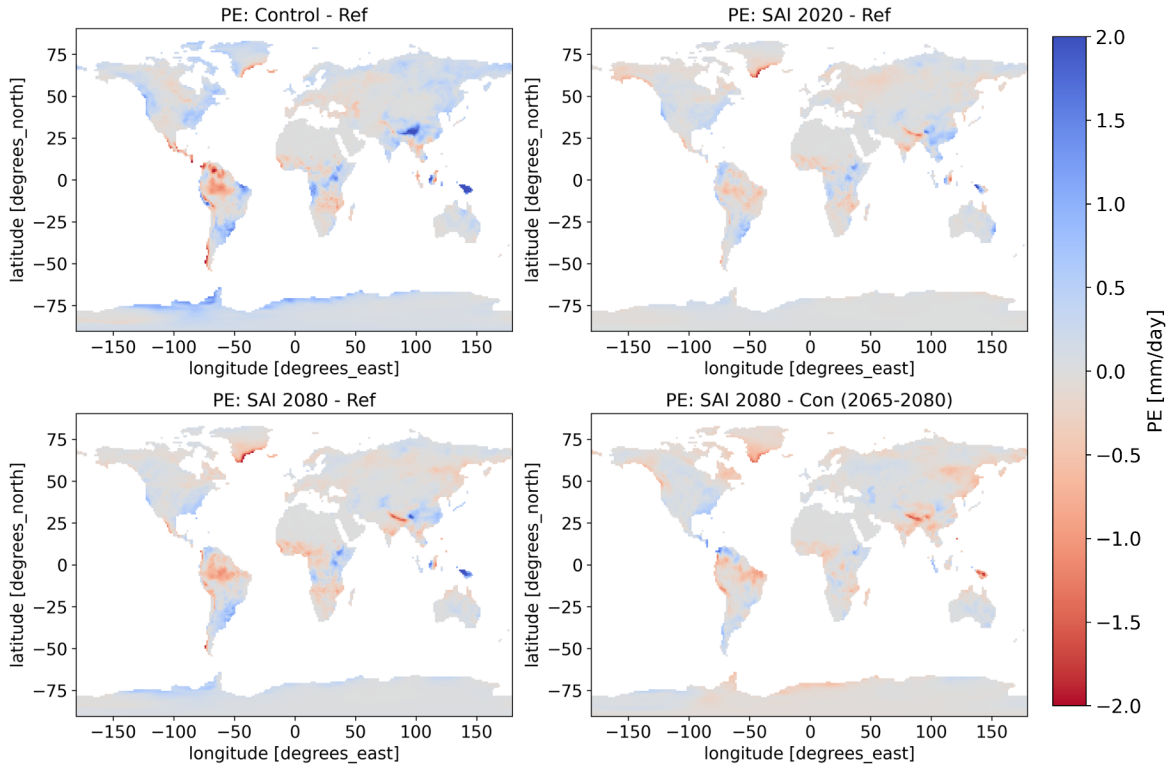

Figure 5: Difference between the 2085-2100 average of every simulation and the reference period (top and bottom-left plots), and between SAI 2080 (2085-2100) and CONTROL (2065-2080) (bottom-right plot) for precipitation minus evaporation.

3.1.2 Simulations' performance

In order to analyze the performance of the three scenarios we established a set of criteria, which determined the assignment of colors. The different colours indicate whether the variables meet the specific conditions or not. As before, we computed the difference between the last 15 years of every simulation with respect to the reference period, and we examined if these differences satisfied the respective criteria. Antarctica and the Caspian lake were masked.

The criteria for acceptable changes vary depending on the variable studied. Namely:

- For TREFHT, we consider differences smaller than 1°C between each simulation and REF as good. This threshold was chosen considering that the reference period already exhibits some warmth, so a negative difference indicates a cooling trend, which can be regarded as a favorable outcome.
- For PRECT and max5, we considered a change as acceptable if the differences were ranging from -5% to +5%. These changes are relatively small and are not

expected to significantly impact the respective regions.

- Lastly, for PE, we accept as good positive differences. This implies that precipitation exceeds evaporation, which is considered favorable.

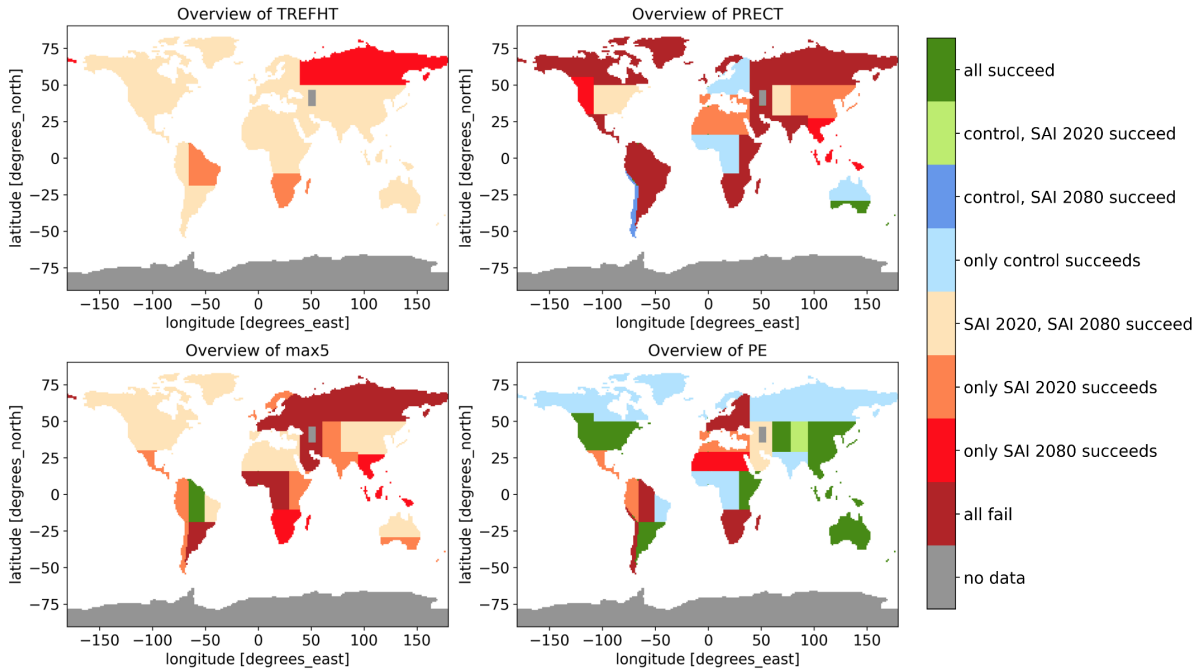

Figure 6: Summary plots for the studied variables. They compare years 2085-2100 with respect to the reference period. The color legend indicates which simulations succeed in fulfilling the criteria and which fail. Antarctica and the Caspian Lake have been masked and left out of the analysis.

The upper-left panel of Figure 6 shows that both SAI simulations meet the aforementioned criteria for the reference height temperature for almost all regions. Only one region has a temperature difference smaller than 1°C exclusively in the SAI 2080 simulation, and only two regions exhibit favorable results only for the SAI 2020 case. CONTROL fails to meet the criteria everywhere.

Looking at the overall analysis of total precipitation (top-right plot), the prevalence of dark red indicates a not so good performance of the simulations. Only one region exhibits a change in PRECT between -5% and +5% for all simulations, and only in two regions SAI 2080 stands out as the only simulation meeting the desired criteria. There are three regions where both geoengineering simulations succeed in fulfilling the criteria, four regions that only experience it with SAI 2020, and only one region where SAI 2020 fails.

Shifting our focus to the lower plots, the left one presents the outcomes for the maximum 5-day precipitation. Interestingly, SAI 2080 appears to achieve the desired criteria in the majority of regions, either as the only successful simulation, together with the CONTROL simulation or alongside the other two simulations. There are six regions in where SAI 2020 is the only favorable simulation, while in the remaining regions all simulations fail to meet the criteria.

Lastly, the bottom-right panel shows the success of all simulations in satisfying the criteria in east Africa, Australia, a significant area of Asia, Argentina and the USA, while failing to do so in South Africa, the Amazon, Chile and Central Europe. Among the regions that do meet the criteria, CONTROL emerges as the most successful scenario, although there are a few regions in where SAI succeeds and CONTROL fails. It is important to note that CONTROL resulting as the most favorable simulation for PE, in general, is because of the chosen criteria for PE, which assumed that increased PE is preferable. Consequently, a simulation that uniformly increases moisture content is more likely to perform better.

3.1.3 Regional analysis

For a more comprehensive examination, we made climatology plots for all the regions, which are available in Appendix 6.1. These plots depict the monthly mean over the last 15 years for every simulation: grey for REF, blue for CONTROL, orange for SAI 2020 and green for SAI 2080. Here we present a selection of plots for various regions, taking into account the following criteria:

- Regions with rich biodiversity and which are ecologically important, such as the Amazon (AMZ), the Congo rainforests (WAF) and the forests of Indonesia and New Guinea (SEA) (Figure 7).
- Regions densely populated, like India (SAS) and east Asia (EAS) (Figure 8).
- Regions that present interesting changes, like Northern and Southern Europe (NEU and MED, respectively), NAS (north Asia) and CGI (Canada, Greenland and Iceland) (Figure 9).

Figure 7 displays the most significant rainforests, as they are areas with important biodiversity. Looking at the Amazon, we see how all three simulations decrease the rain intensity in comparison to the reference, implying that precipitation-wise deploying

SAI does not contribute to a better outcome over this area. Conversely, the simulations over Indonesia show the opposite trend, where all scenarios show increased precipitation, excluding the month of July. The west Africa region presents a diverse pattern, but overall we can observe how SAI 2080 dries the most, except in July.
In terms of temperature, only the region over Indonesia presents the expected trend. CONTROL demonstrates higher temperature values, while both SAI simulations present similar values in relation to REF (it is worth noting, however, that during the summer months temperatures with geoengineering are slightly higher than reference). Notably, in the Amazon and in the Congo regions, temperature increases in comparison to REF even when SAI is deployed.

In Figure 8 we can see the climatology plots for two of the most populated regions. Both India and the eastern part of China present a similar temperature pattern. The CONTROL simulation exhibits higher temperatures while the geoengineering cases have closer values to the reference period. Note how in India the SAI simulations project higher temperatures than REF during the summer. Still in India, CONTROL significantly amplifies the intensity of the rainy season, while SAI results in a slightly drying effect. This means that in CONTROL the monsoons intensify, while in SAI they decrease their intensity. Similarly, in the east of China precipitation increases with CONTROL but remains comparable to REF or slightly lower with SAI.

Finally, Figure 9 shows some regions with interesting changes. In Northern Europe, for example, precipitation gets a pronounced seasonal cycle under CONTROL (wetter winter and drier summer compared to REF). When deploying SAI, winters stay similar to REF but summers decrease their precipitation. Additionally, temperature in SAI 2080 is lower than in the reference period, supporting our previous findings that showed an overcooling over that area in SAI 2080 (see Section 4.3).
In Southern Europe, precipitation drastically decreases in CONTROL. Deploying SAI slightly increases rainfall, but the precipitation levels still remain below the reference values.
Finally, for both Northern Asia and the region over Canada, Greenland and Iceland, precipitation increases considerably for CONTROL in comparison to the reference period during all year, except in summer. Deploying SAI leads to less precipitation, both for SAI 2020 and SAI 2080. Temperature-wise, we observe how in winter the increase

for the high emission scenario is larger in comparison to the increase in summer, probably due to polar amplification.

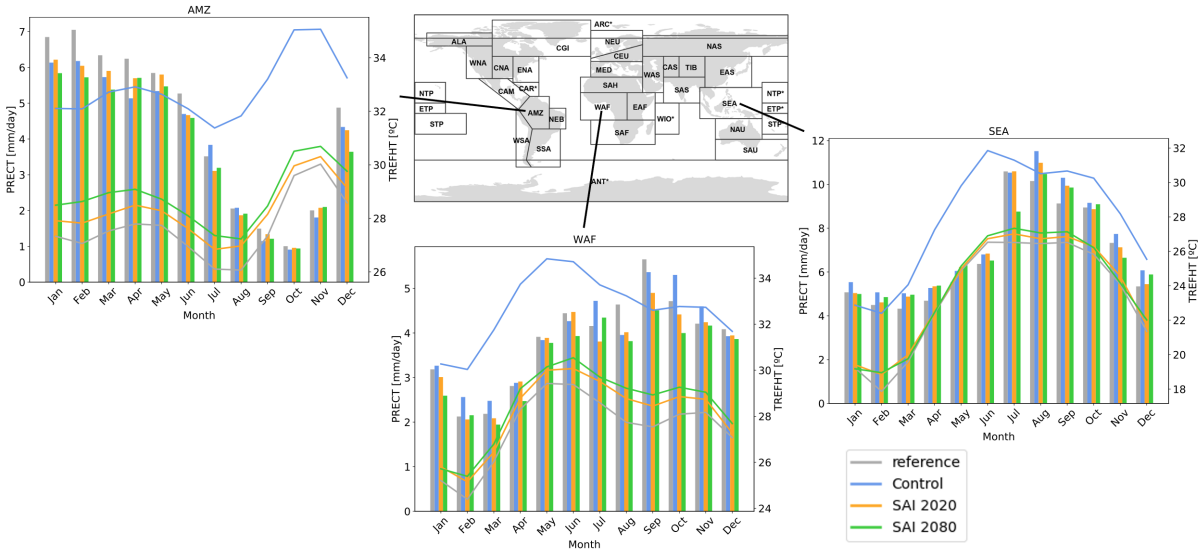

Figure 7: Climatology plots for the ecologically important regions. The bars show the total precipitation (left axis) and the lines the reference height temperature (right axis).

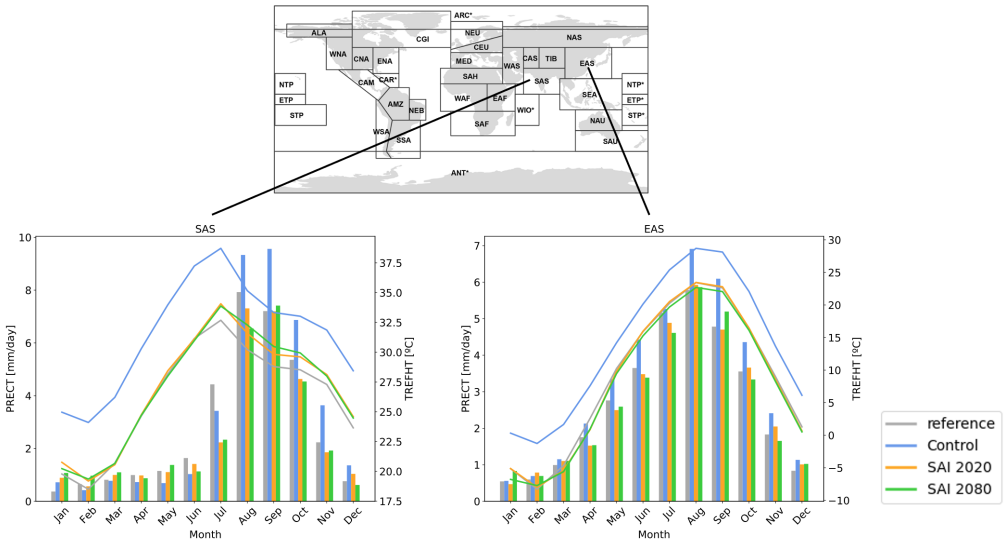

Figure 8: Climatology plots for the most populated regions. The bars show the total precipitation (left axis) and the lines the reference height temperature (right axis).

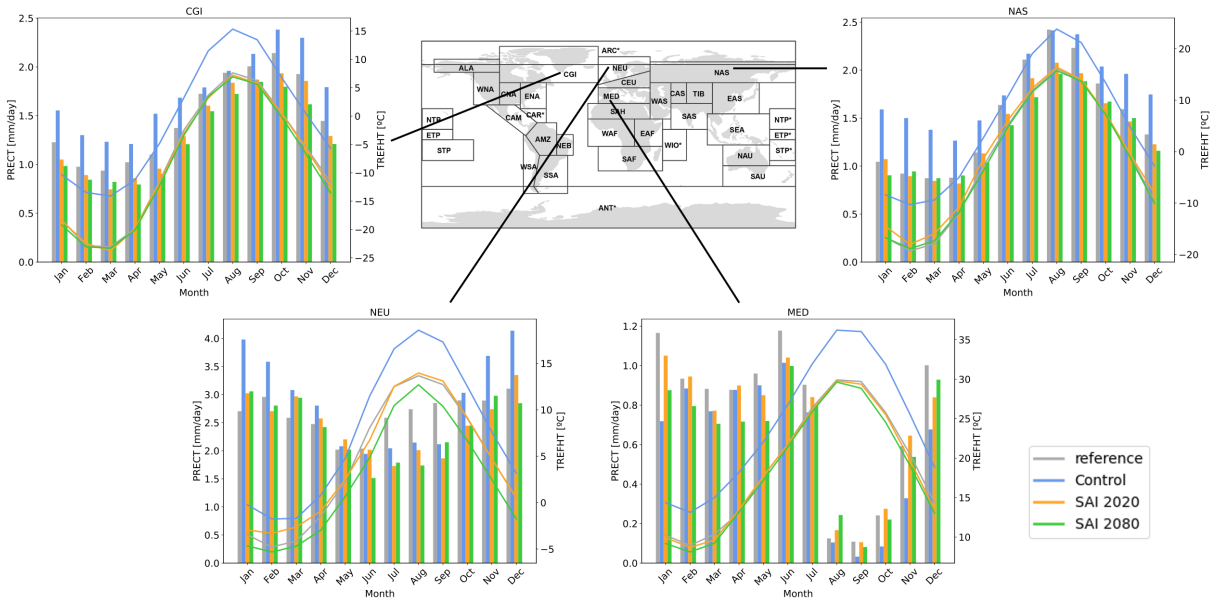

Figure 9: Climatology plots for interesting regions. The bars show the total precipitation (left axis) and the lines the reference height temperature (right axis).

3.1.4 Simulations' comparison

In order to directly compare the different scenarios, we made exacerbation plots for the different variables. These type of plots are particularly useful in evaluating the effectiveness of interventions (in this case, of SAI), as they can demonstrate whether a particular measure has succeeded in reducing or mitigating exacerbations over time.

Again, we compared the last 15 years of every simulation with respect to the reference period, and the results can be seen in Figure 10. The first two columns of the figure show the comparison between CONTROL and the two SAI simulations, whereas the final column compares the two geoengineering scenarios between them. Every point represents a grid cell. We also made seasonal exacerbation plots (i.e., for the months of December-January-February (DJF) and June-July-August (JJA)), which are included in Appendix 6.2.

When looking at Figure 10, a striking similarity becomes apparent for the four variables. All the plots exhibit the same pattern, characterized by a spot that is wider than it is tall in the "SAI 2020 vs Control" and "SAI 2080 vs Control" cases, and a diagonal spot in the "SAI 2080 vs SAI 2020" plot. The shape of the two first columns shows how the CONTROL simulation has the data more spread out than the geoengineering

scenarios (see Section 4.1 for interpretation). In Figures 10b, 10c and 10d the spot is noticeably positioned at the center, meaning that the changes under CONTROL are smaller than in Figure 10a.

In each of the subplots, a few data points deviate from the main cluster, indicating the presence of extreme conditions in certain regions. To identify these specific regions, we have to look at the figures presented in Section 3.1.1. After comparing them, one can deduce that the bottom-left "tail" in the last plot of Figure 10a corresponds to Greenland, where there is an overcooling in SAI 2080 in comparison to SAI 2020 (see Section 4.3). Similarly, the outliers in the right-central part of the first two plots in Figures 10b and 10c represent Antarctica and Greenland, showing that these regions receive more rainfall in CONTROL than in SAI. The last plot of these same figures accounts for the Arabic peninsula, which has more precipitation for SAI 2080 than for SAI 2020. Lastly, the right-central outliers in the first two columns of Figure 10d can be attributed to the region over Bangladesh, Indonesia and Papua New Guinea, which present higher values of PE for CONTROL than for SAI.

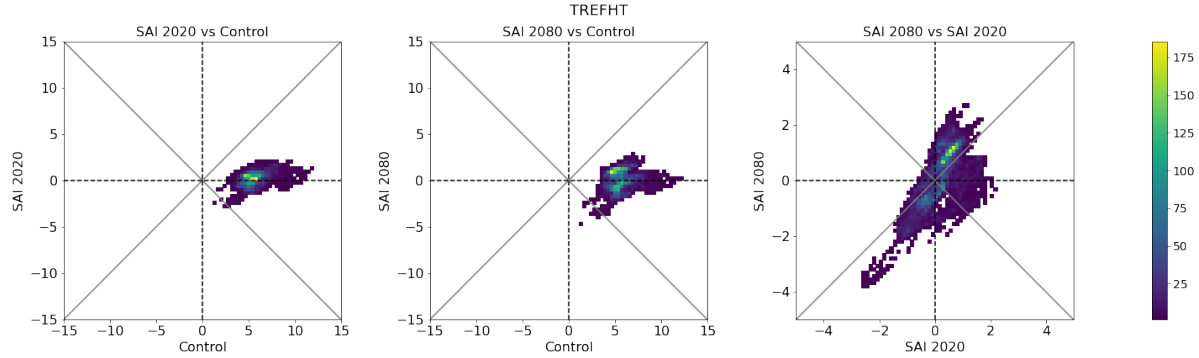

(a) 2085-2100 average exacerbation plot for TREFHT.

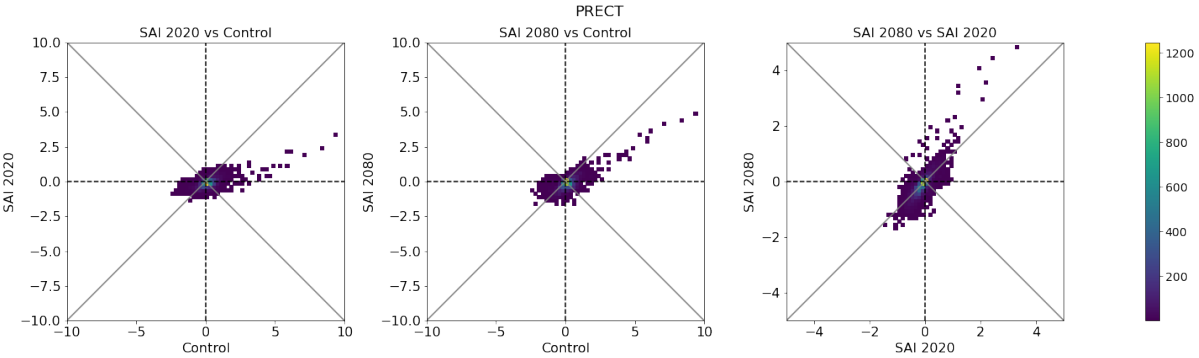

(b) 2085-2100 average exacerbation plot for PRECT.

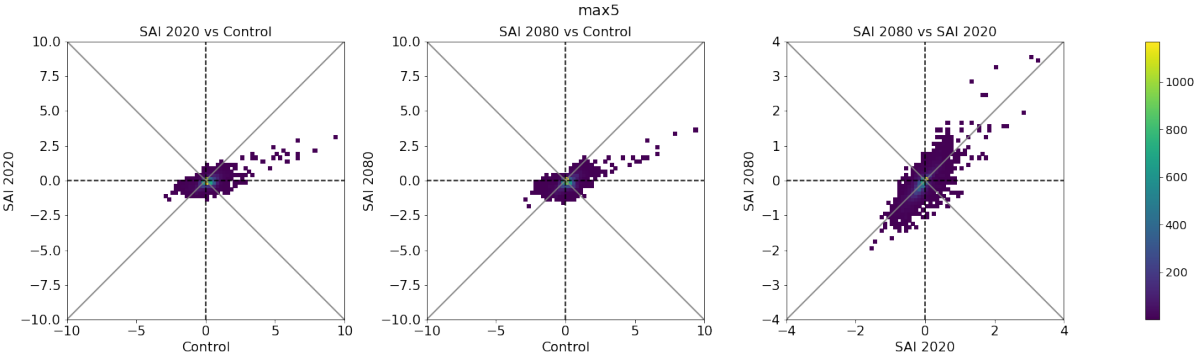

(c) 2085-2100 average exacerbation plot for max5.

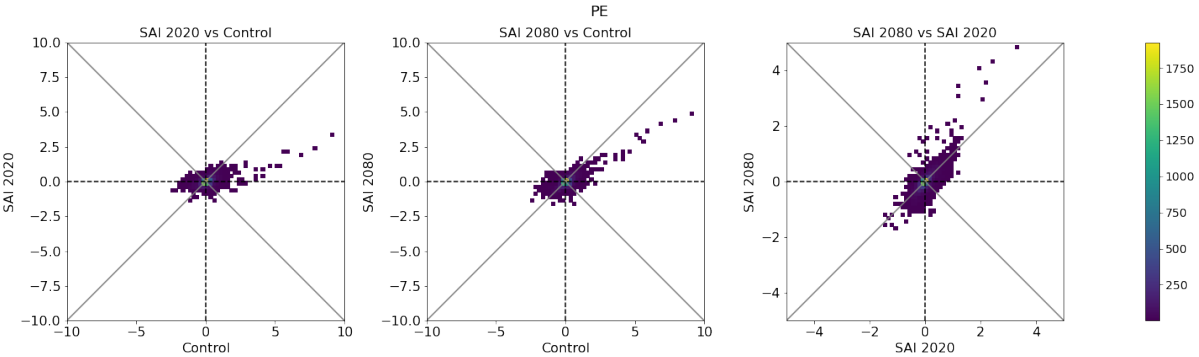

(d) 2085-2100 average exacerbation plot for PE.

Figure 10: Exacerbation plots. They compare the last 15 years with respect to the reference. Every point represents a grid cell.

3.2 Ecological analysis

3.2.1 Köppen climate classification

As explained in Section 2.3.2, the Köppen classification is a way to divide climates based on the monthly temperature and precipitation patterns, thus providing valuable insights into regional climate variations. Within this section, we present the results derived from the three different simulations, employing a time range of 20 years instead of 15. Consequently, the considered reference period spans from 2015 to 2035 and the analysis for the simulations goes from 2080 until 2100.

Figure 11 shows the Köppen climate diagrams for the reference period (top-left), the CONTROL simulation (top-right), SAI 2020 (bottom-left) and SAI 2080 (bottom-right). Due to the applied land mask, some coastal areas, including Japan, Madagascar, part of Indonesia, Italy or part of Central America, are not included in the plots.

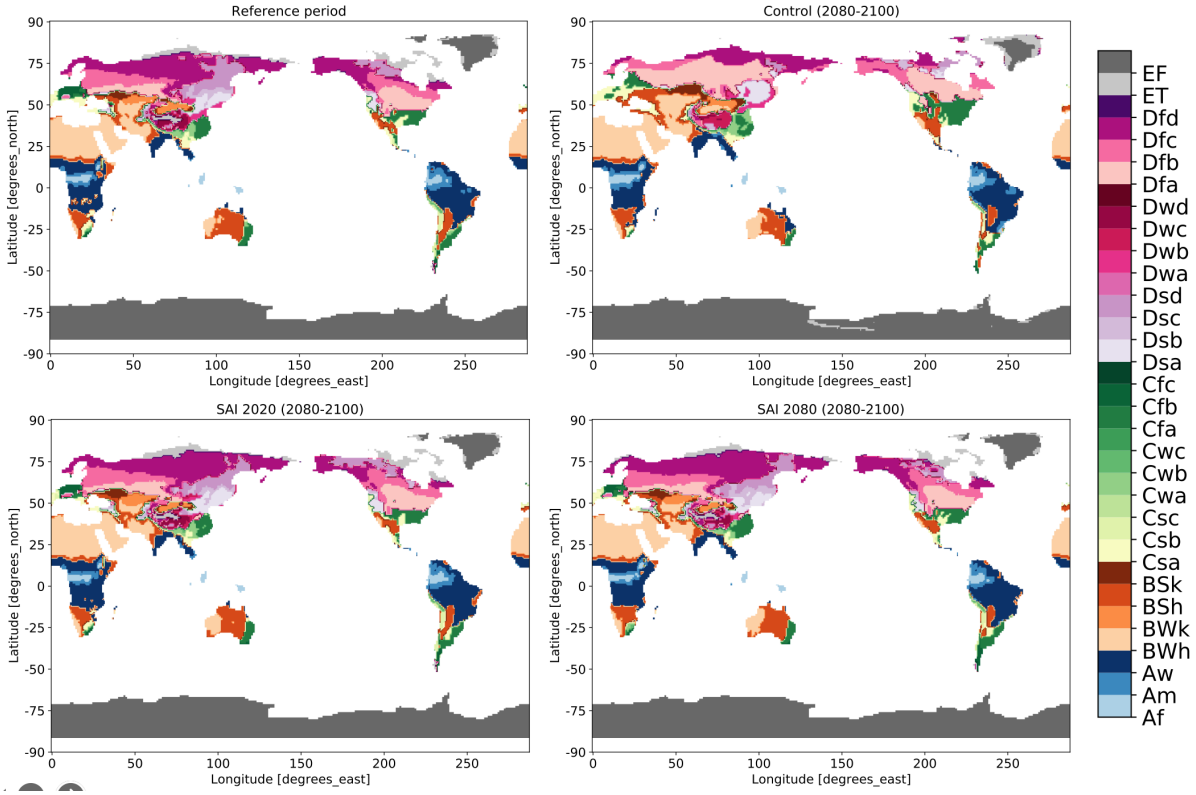

Figure 11: Köppen climate classification for every scenario. The reference period goes from 2015 to 2035. The simulations show the average between 2080 and 2100. The color legend indicates the groups presented in Section 2.3.2.

Figures 12 and 13 provide a closer examination of the regions of Asia and Canada and

Greenland, respectively. These figures offer a more detailed picture, allowing for a clearer understanding of the observed trends.

When comparing the two upper plots in Figure 11, it becomes evident that the most significant changes occur in the high latitudes of the NH, specially in Russia, Alaska and northern Canada (see Figures 12 and 13 for a closer look). These regions undergo a transition from Dfc (subartic climate, so continental no dry season and cold summer) to Dfa and Dfb (continental no dry season and hot and warm summer), indicating warmer temperatures. Also, the region with continental dry and cold summer (Dsc) disappears in the CONTROL simulation. Similarly, Greenland transforms from EF (ice caps) to ET (tundra), reflecting the shift towards higher temperatures. Central and eastern Europe go from Cfb (oceanic climate, so temperate no dry season and cold summer) to a hot-summer mediterranean climate (Csa), again as a result of increased temperatures. Additionally, there are some minor changes in South Africa, South America and Australia, also influenced by higher temperatures.

Turning our attention to the two lower plots in Figure 11, we can observe that they closely resemble the reference plot. This comes as no surprise, as we have already seen in Figures 2 and 3 that the geoengineering scenarios do not differ significantly from the reference period. In the SAI 2020 simulation, the most notable differences occur in Alaska and Greenland, where mediterranean-influenced subarctic climate (Dsc) expands while the extremely cold subarctic climate decreases (Dfd) (see Figure 13 for a closer look).

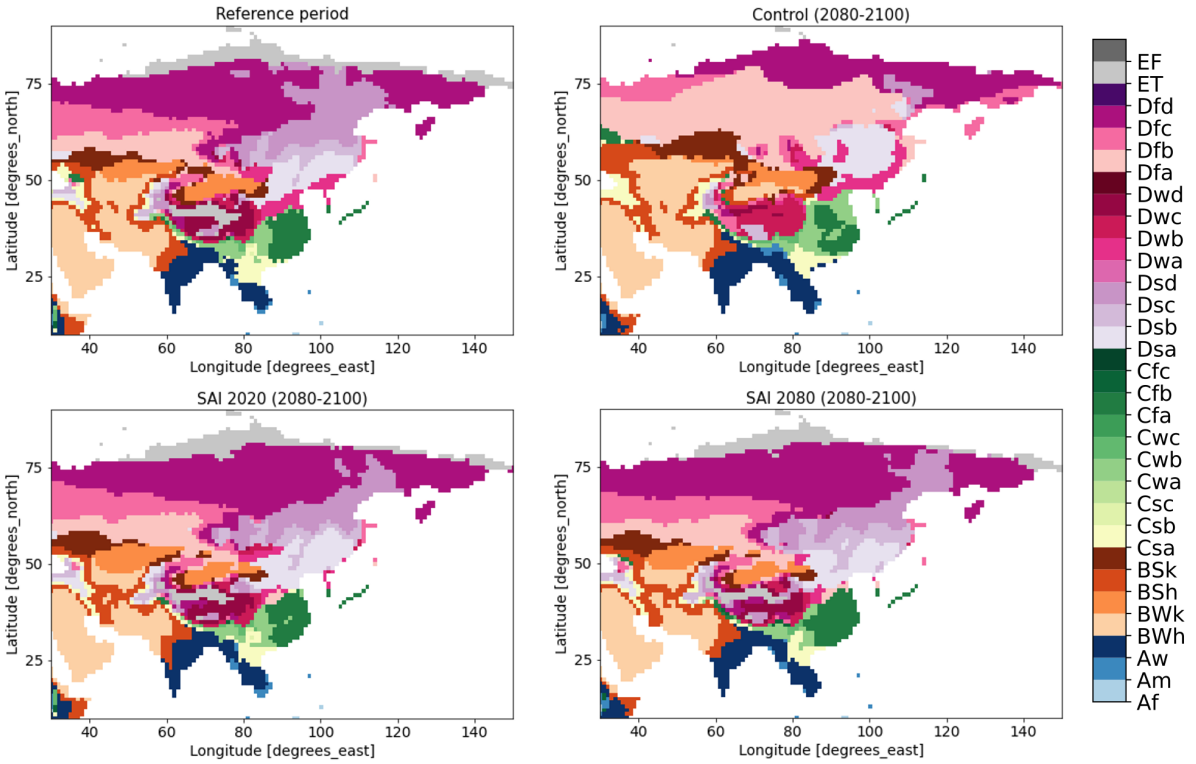

Figure 12: Köppen climate classification for Asia. The reference period goes from 2015 to 2035. The simulations show the average between 2080 and 2100. The color legend indicates the groups presented in Section 2.3.2.

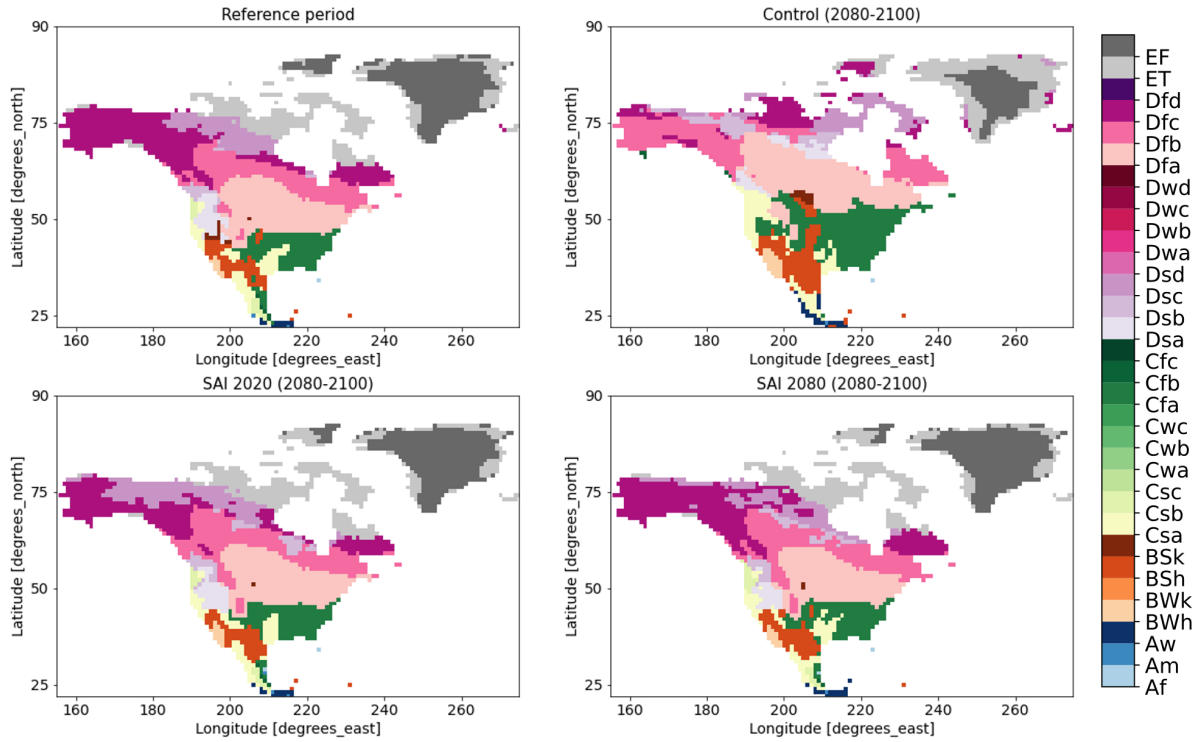

Figure 13: Köppen climate classification for Canada and Greenland. The reference period goes from 2015 to 2035. The simulations show the average between 2080 and 2100. The color legend indicates the groups presented in Section 2.3.2.

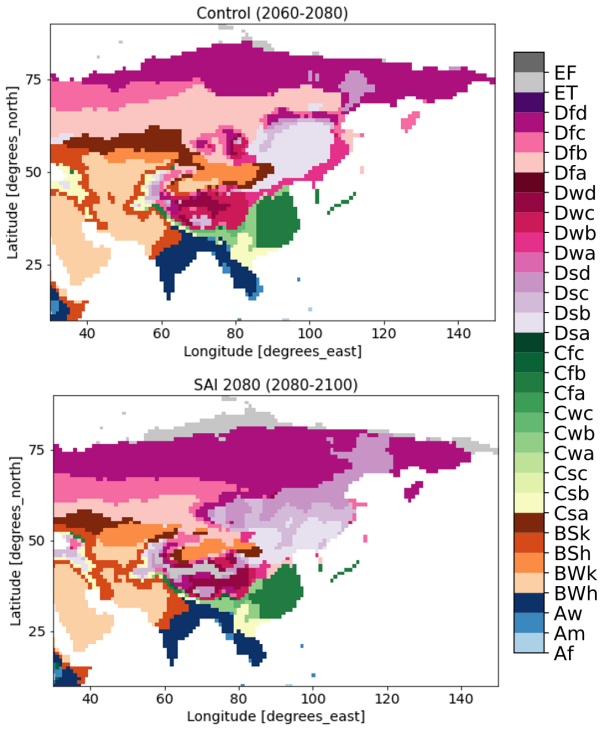

Figure 14: Köppen climate classification for Asia. The upper plot shows CONTROL from 2060 to 2080, and the bottom one SAI 2080 for 2080 until 2100. The color legend indicates the groups presented in Section 2.3.2.

For a better interpretation of the SAI 2080 plot, it is useful to compare it with the CONTROL simulation during the years previous to the implementation of SAI (i.e., from 2060 until 2080). Figure 14 demonstrates how SAI 2080 effectively reverts the climate to the conditions observed in the reference period over Asia (see Figure 12 for comparison).

This observation proves that SAI 2080 is able to restore the climate, at least within that particular region. The comparison of Canada and Greenland is shown in Appendix 6.3.

3.2.2 Migration lines

While the Köppen climate plots effectively present regional climate shifts, they do not provide insights into the specific changes in individual meteorological variables or variations in extreme events. They also fail in showing the speed at which these climate movements are occuring. To address these aspects, we have generated migration lines plots for the warmest and coldest month (Figures 15 and 16, respectively) and for the wettest and driest month (Figures 17 and 18, respectively). Understanding the rate at which climate is changing proves valuable as it allows for a comparison with the speed at which ecosystems can migrate. This knowledge helps determine whether species can move fast enough to ensure their survival (see Section 4.2).

Again, for both the reference period and the studied simulations, a time span of 15 years was chosen. Therefore, the reference period encompasses the years 2015 to 2035, while the simulations cover the period from 2085 to 2100. The top-left plot in each

of the figures illustrates the position of the studied isolines (also known as contour lines) corresponding to the reference period. In the remaining three subplots, the isolines show the location of the respective extreme events and are color-coded based on the difference between their positions in the simulation under consideration and their positions in the reference period. The closer the two isolines are, the darker the color. Only the isolines covering the bigger areas were taken into account for the analysis.

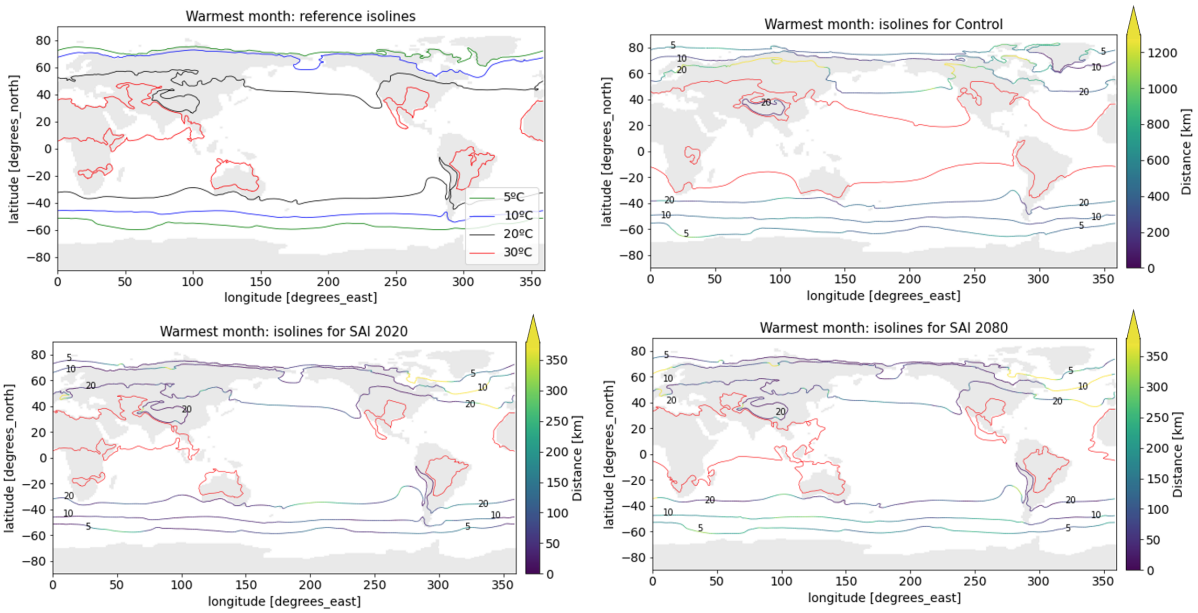

Figure 15: 5ºC, 10ºC, 20ºC and 30ºC isotherms during the warmest month. The considered time span is from 2085 to 2100.

Figure 15 illustrates the isotherms corresponding to the warmest month. We observe that the isolines travel the most in the CONTROL simulation, indicating that this scenario undergoes the most significant alterations. Among the two geoengineering scenarios, the largest displacements occur in the SH during SAI 2080.

The calculations for the distances traveled by the 30ºC isotherm were omitted due to their big magnitude in comparison to the other distances. Instead, only the isolines (depicted as red lines) were plotted. In REF and in SAI 2020 the 30ºC isotherms are limited to specific regions such as Australia and the mid-latitudes in the NH. However, the isolines for the same temperature in CONTROL extend across the entire globe. Consequently, this expansion of the isotherms results in a warmer warmest month for various regions, including South Africa or Australia. Still in the CONTROL simulation, the 30ºC isotherm crosses the Mediterranean. Furthermore, in SAI 2080 the area

covered by the 30ºC isotherm expands considerably, particularly over Africa.

Examining the high latitudes in the NH, one can observe that in REF and both SAI simulations, the 5ºC isotherm encircles the southern region of Greenland, while in CONTROL it passes above it, indicating a warming trend. Finally, it is worth noting that The Himalayas and The Andes represent a cold spot, primarily because of their elevated altitudes and steep topography, which make it difficult to change these mountain chains temperature.

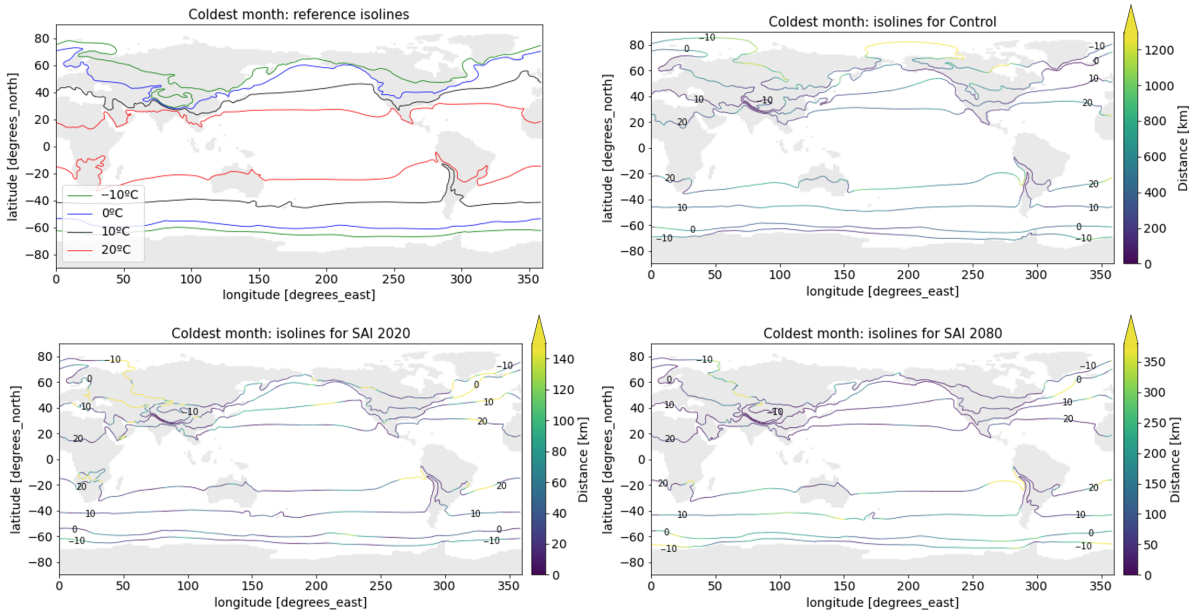

Figure 16: -10ºC, 0ºC, 10ºC and 20ºC isotherms during the coldest month. The considered time span is from 2085 to 2100.

Moving on to Figure 16, it represents the isotherms for three distinct values during the coldest month. Similarly, the greatest displacements occur in CONTROL, while SAI 2020 exhibits the smallest variations. Analyzing the movement of the isotherms, several observations can be made. Firstly, the -10ºC isotherm in the NH ascends, leading to increased warming in northern Canada. Secondly, as the 20ºC isotherm rises in the NH, the southern part of the Arabic peninsula warms. Lastly, the descent of the 20ºC isotherm in the SH results in warming in South Africa and in the northern part of Australia. The irregularities observed in the high latitudes of the NH for the -10ºC could be attributed to sea ice melting, which results in reduced albedo and consequently higher temperatures in the area.

The close aligment of the isolines with coastlines (particularly noticeable in eastern Asia and western USA and Canada) can be attributed to the difficulty in crossing these boundaries. During an extreme event, such as the coldest month in this case, the temperature gradient between the land and the ocean is significant, making it challenging for the isolines to transition between the two.

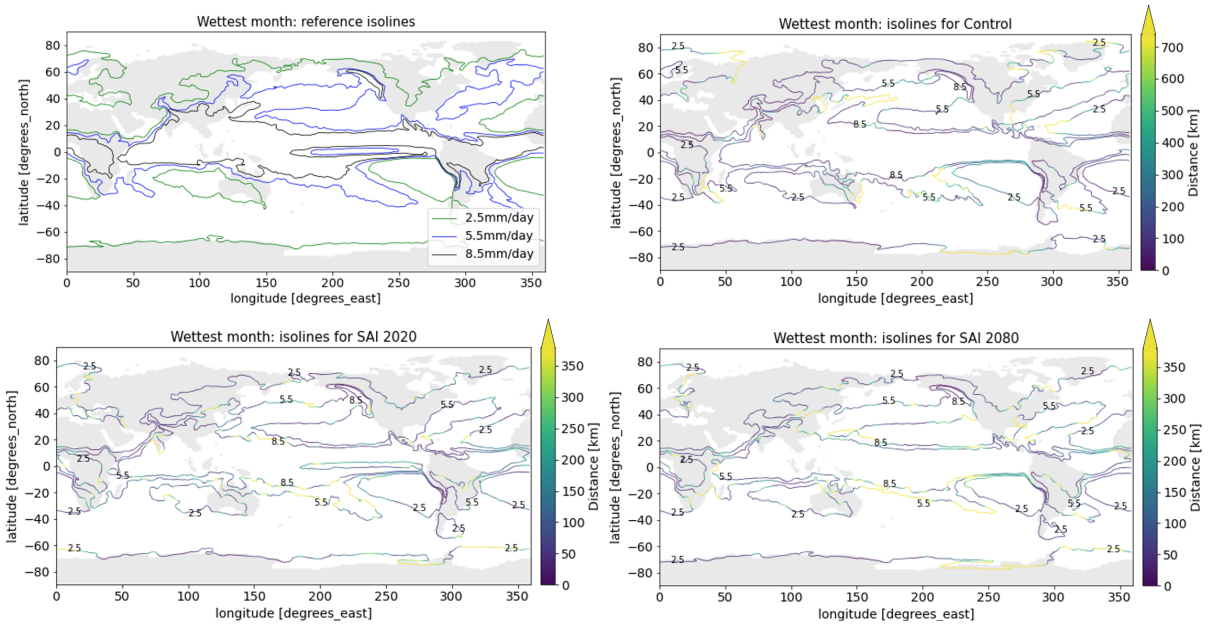

Figure 17: 2.5mm/day, 5.5mm/day and 8.5mm/day precipitation isolines during the wettest month. The considered time span is form 2085 to 2100.

Figure 17 shows the precipitation isolines during the wettest month for three different values. Comparing the changes observed in CONTROL with those observed during the warmest and coldest months, it can be deduced that the displacements in precipitation are smaller than those in temperature. Additionally, the most substantial alterations in precipitation occur over the ocean.

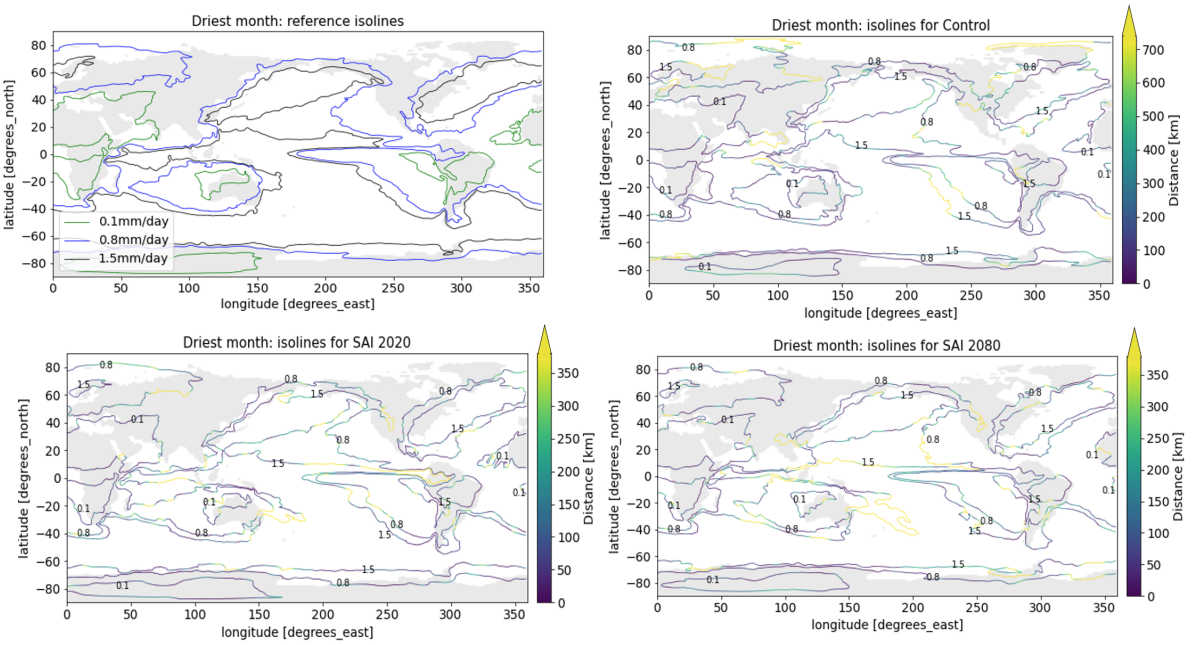

Figure 18: 0.1mm/day, 0.8mm/day and 1.5mm/day precipitation isolines during the driest month. The considered time span is form 2085 to 2100.

Finally, Figure 18 presents the precipitation isolines during the driest month. This plot confirms not only that the changes in precipitation are smaller compared to temperature for CONTROL, but also that the largest variations happen over the ocean. However, the magnitude of these changes is larger than for the changes during the wettest month, as indicated by the lighter colors in comparison to Figure 17. As an example, we can see that precipitation increases in the area between 60ºN-80ºN, 0ºE-100ºE in CONTROL, result of the northward shift of the 0.8mm/day isoline.

4 Discussion

4.1 Performance of the geoengineering simulations

All the global maps presented in Section 3.1.1 demonstrate that the geoengineering scenarios effectively maintain values closer to reference in comparison to CONTROL. In other words, we proved that temperature and precipitation decrease if SAI is deployed relative to CONTROL, which matches with what other studies found (Irvine et al., 2019; Tilmes et al., 2020; Pamplany et al., 2020; de Coninck et al., 2020; Tracy et al., 2022). This decreasing trend is deduced by the weaker colors shown in the comparison plots between the SAI scenarios and the reference period. This fact is further corroborated by Figure 6, which shows that the regions where the SAI simulations successfully meet the established criteria outnumber the regions where CONTROL does it.
The first two columns of the figures shown in Section 3.1.4 further reinforce this notion. As previously mentioned, the spatial extent is wider than it is taller, indicating that the changes in the CONTROL simulation are bigger compared to the SAI cases. Consequently, this further proves the worse performance of the CONTROL simulation in keeping values close to the reference (in comparison to the SAI simulations). Finally, both Figure 11 and Section 3.2.2 show how the changes in the climate and its extreme events are smaller under the geoengineering simulations than in a high emission scenario.

Regarding the comparison between the two geoengineering simulations, Figure 6 provides valuable insights. In terms of the reference height temperature, SAI 2020 successfully meets the criteria in all regions except one, while SAI 2080 accomplishes this in all regions except for two. Concerning precipitation, SAI 2080 outperforms SAI 2020, achieving success in more regions for both total precipitation and maximum-5day precipitation. Lastly, for precipitation minus evaporation, both simulations perform correctly, meeting the criteria in all the regions except for three in SAI 2020 and two in SAI 2080.

4.2 Ecosystems' adaptation

As stated in Section 3.2.2, by knowing the pace at which climate features are moving it possible to know if species have a chance to survive. Figure 19 shows the maximum

speed at which species can move in kilometers per decade. For example, we can observe how while trees and plants are the slowest group of species, with nearly 0km per decade, split-hoofed and carnivorous mammals are the fastest, as they can move at 90 and 60km per decade, respectively.

These velocities can be compared to the ones presented in Section 3.2.2. In this context, I will only focus on the examination of the changes during the warmest month, although the discussion can be extended to the remaining three cases from that section. Considering the most extreme case in Figure 15, we see how the isotherms move more than 1200km, equivalent to around 20km/year. By comparing this velocity with the migration speeds shown in Figure 19, it can be deduced that only freshwater mollusks and the split-hoofed and carnivorous mammals would survive, as they are the only ones able to adapt at a sufficient rate.

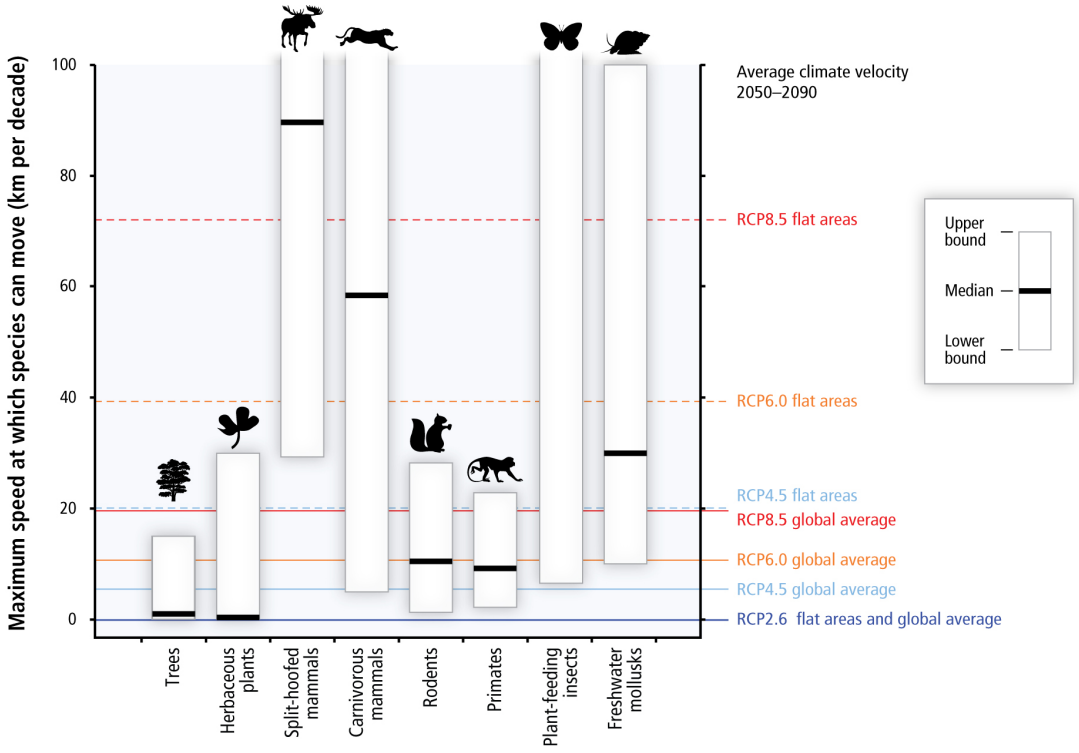

Figure 19: Maximum speed at which species can move in km per decade. The thick black line indicates the median velocity, while the columns account for the upper and lower bounds. The coloured horizontal lines represent the average climate velocity between 2050 and 2090 for different RCP scenarios. Source: Field et al., 2014.

Finally, and still discussing the warmest month (Figure 15), it is important to emphasize the significance of the SAI 2080 plot. Although the distances travelled by the isolines resemble those of SAI 2020, we must bear in mind that in SAI 2080 the climate

has warmed, and when SAI is implemented, conditions are reversed. Consequently, if certain species have already adapted to a warmer climate or are in process of doing so, reverting to past conditions can be harmful for them. Therefore, it can be concluded that SAI 2080 has the potential to destroy certain ecosystems.

4.3 Influence of SAI on the AMOC

The Atlantic Meridional Overturning Circulation (AMOC) is a system of ocean currents in the Atlantic Ocean responsible for bringing warm water north and cold water south (NOAA, n.d.). In a simplified manner, this circulation process works as follows: it begins with warm and salty water moving towards the North Atlantic, where it cools. As this cooling is taking place, waters sinks down and flows southwards in the deeper layers. Therefore, the driving force behind the AMOC are the differences in temperature and salt content.

The AMOC's significance extends beyond oceanic dynamics, as it also influences global climate patterns: it is thought to moderate the climate of northern and western Europe, which affects Eurasia as well (Hirschi et al., 2020). Changes in the heat and salt transported by the AMOC can lead to various climatic effects, such as alterations in tropical cyclone frequency and intensity and changes in monsoonal rainfall in Africa and India (Xie et al., 2022). Hence, any modifications to the AMOC caused SAI have the potential to generate significant societal impacts. Consequently, understanding how the AMOC will evolve in the future is crucial.

In Figure 2 we saw how Greenland experiences the least warming across all three scenarios, with even a cooling effect observed in the geoengineering simulations, particularly in the case of SAI 2080. This observation suggests a weakening of the AMOC in the late geoengineering case, as reduced warming implies less heat transport to the NH (Daniel Pflüger, 2023, *in prep.*). Further evidence for this can be found in the bottom-left subplot of the same figure, where the implementation of SAI 2080 results in greater warming in the SH compared to the NH. Continuing in this line, the climatology of Northern Europe in Figure 9 depicts lower temperature in SAI 2080 than in the reference period, which again proves the reduced heat transport to the NH. Finally, the third plot of Figure 10a clearly illustrates the significant overcooling effect in SAI 2080 when compared to SAI 2020, seen as a tail in the bottom-left region. These points

represent the region around Greenland.

4.4 Limitations and future research

Here we openly discuss the limitations of our research and the factors that could have influenced our results. By acknowledging these limitations, we aim to present a balanced interpretation of our finding. We also present a simplified overview of what would be needed in future research.

The first limitation of the current project is that rather than running a climate model ensemble, we only relied on a single model. Ensembles allow for quantifying uncertainties and giving a more robust understanding of the projected climate changes, so using only one model is not ideal. Also, models often have biases or systematic errors in simulating specific aspects of the climate system, making it challenging to assess their performance and credibility when restricted to a single model.

The second limitation that questions the reliability of our results is the short time span covered by our simulations, which include less than one century. This limited duration fails to capture not only long-term climate trends (like multi-decadal oscillations or slow responses to external forcing), but also low-frequency variability, such as ocean circulation patterns like the AMOC. Furthermore, short-term simulations are very sensitive to the initial state of the climate system, meaning that even small differences in the initial conditions can lead to significant variations in the simulated climate over time.

Lastly, the simulations analysed in this project do not represent realistic scenarios. Instead, they explore extreme cases designed to examine the behavior of the climate system when deploying SAI.

Considering the limitations listed above, we believe future research on this topic should prioritize the use of a climate model ensemble and extend the duration of the simulations. Also, we recommend the exploration of less extreme scenarios to study more plausible future situations. In the context of environmental research, we strongly encourage the integration of an ecological model, as it allows for a more realistic repre-

sentation of the complexity and variability of natural systems. In addition, this kind of model can simulate and predict the responses of species not only to environmental changes, but also how organisms may be affected by different scenarios or interventions. All in all, we encourage for future collaboration between ecologists and climate scientists for investigating what consequences for ecological systems can the deployment of SAI have (Zarnetske et al., 2021).

5 Conclusion

The main focus of this project was to investigate the impact of different scenarios on important meteorological variables, like temperature and precipitation. Section 3.1 extensively addresses this research question, providing different perspectives on the changes in reference height temperature, total precipitation, maximum 5-day precipitation and precipitation minus evaporation that will result from geoengineering deployment. We saw how both temperature and precipitation are expected to decrease for SAI 2020 and SAI 2080 in comparison to CONTROL, with some exceptions like Greenland.
The decrease in temperatures can be perceived as a positive output, as it proves the mitigation of the warming trend. However, if the magnitude of this decrease is very strong, it may introduce additional challenges. Similarly, a reduction in precipitation may not be ideal, particularly in regions already experiencing limited rainfall.

Another question we tried to answer was whether SAI has the potential to bring the future climate close to conditions similar to those observed during the reference period. And the answer is "yes". This affirmative response can be supported by two main arguments: the first one, by the results shown in Section 3.2, which proved how even SAI 2080 is able to partially restore the climate to how it was during the reference period. The second argument is that throughout the project, we consistently saw that the differences between the geoengineering simulations and the reference period were significantly smaller than those between CONTROL and the reference period. This emphasises the efficacy of SAI in climate restoration, even if implemented as late as 2080. Therefore, deploying SAI proves more advantageous than continuing with current emission practices.
Whether it is better to start SAI now (in 2020) or wait until 2080 is not straightforward to answer, as it depends on the specific variable in question.

Concerning the potential ecological implications, we saw how SAI 2080 has the capacity to harm certain ecosystems due to the reversal of the climatic conditions. This presents a significant concern for species that have already adapted to a warmer climate, as the implementation of SAI in 2080 can introduce adverse effects by changing the environmental conditions they have adapted to.

Finally, we conclude that further research has to be made in the interaction of SAI and ecosystems. This will enable us to gain valuable insights that can inform future potential deployments of SAI.

Acknowledgements

I would like to thank my first supervisor, Claudia Wieners, for her guidance throughout the whole project. I also want to thank Daniel Pflüger, my daily supervisor, for his endless patience in debugging my code. Both of them have made themselves available to answer my questions and have trusted me since the beginning, and I am very grateful.

I would also like to thank Jessica Gurevitch (Distinguished Professor and Department Head of Purdued University) and Cheryl S. Harrison (Assistant Professor at Louisiana State University) for dedicating part of their time to this project. Their contributions and expertise in the field of ecology have greatly enhanced my work, and I appreciate their commitment.

Bibliography

AR5 reference regions. (n.d.). https://www.ipcc-data.org/guidelines/pages/ar5_regions.html

Biernmann, F., & Möller, I. (2019). Rich man's solution? climate engineering discourses and the marginalization of the global south. *International Environmnental Agreements: Politics, Law and Economics 19, p. 151-167*. https://doi.org/https://doi.org/10.1007/s10784-019-09431-0

Crutzen, P. (2006). Albedo enhancement by stratospheric sulfur injections: A contribution to resolve a policy dilemma? *Climatic Change, 77, p. 211-219*. https://doi.org/https://doi.org/10.1007/s10584-006-9101-y

Cui, D., et al. (2021). Observed and projected changes in global climate zones based on köppen climate classification. *WIREs Climate Change, Vol 12, Issue 3*. https://doi.org/https://doi.org/10.1002/wcc.701

Danabasoglu, G., et al. (2020). The community earth system model version 2 (CESM2). *Journal of Advances in Modelling Earth Systems, Vol 12, Issue 2*. https://doi.org/https://doi.org/10.1029/2019MS001916

de Coninck, H., et al. (2020). Strengthening and implementing the global response. In V. Masson-Delmotte, P. Zhai, H.-O. Pörtner, D. Roberts, J. Skea, P. Shukla, A. Pirani, W. Moufouma-Okia, C. Péan, R. Pidcock, S. Connors, J. Matthews, Y. Chen, X. Zhou, M. Gomis, E. Lonnoy, T. Maycock, M. Tignor, & T. Waterfield (Eds.), *Global warming of 1.5°c. an IPCC special report on the impacts of global warming of 1.5°c above pre-industrial levels and related global greenhouse gas emission pathways, in the context of strengthening the global response to the threat of climate change, sustainable develptment, and efforts to eradicate poverty* (pp. 313–444). Cambridge University Press.

Feng, S., et al. (2011). Evaluating observed and projected future climate changes for the arctic using the köppen-trewartha climate classification. *Climate Dynamics 38, 1359-1373*. https://doi.org/https://doi.org/10.1007/s00382-011-1020-6

Field, C., et al. (2014). Summary for policymakers. In C. Field, V. Barros, D. Dokken, K. Mach, M. Mastrandrea, T. Bilir, M. Chatterjee, K. Ebi, Y. Estrada, R. Genova, B. Girma, E. Kissel, A. Levy, S. MacCracken, P. Mastrandrea, & L. White (Eds.), *Climate change 2014: Impacts, adaptation, and vulnerability. part a: Global and sectoral aspects. contribution of working group ii to the fifht assessment report of the intergovernmental panel on climate change* (pp. 1–32). Cambridge University Press.

Hirschi, J., et al. (2020). The atlantic meridional overturning circulation in high-resolution models. *Journal of Geophysical Research: Oceans, Vol 125, Issue 4*. https://doi.org/https://doi.org/10.1029/2019JC015522

Hulme, M. (2012). Climate change: Climate engineering through stratospheric aerosol injection. *Sage Journals, Vol 36, Issue 5*. https://doi.org/https://doi.org/10.1177/0309133312456414

Irvine, P., et al. (2019). Halving warming with idealized solar geoengineering moderates key climate hazards. *Nature Climate Change, 9, p. 295-299*. https://doi.org/https://doi.org/10.1038/s41558-019-0398-8

Iturbide, M., et al. (2020). An update of IPCC climate reference regions for subcontinental analysis of climate model data: Definition and aggregated datasets. *Earth System Science Data, Vol 12, Issue 4, p. 2959–2970*. https://doi.org/https://doi.org/10.5194/essd-12-2959-2020

Kravitz, B., et al. (2011). The geoengineering model intercomparison project (geoMIP). *Atmospheric Science Letters, Vol 12, Issue 12, p. 162-167*. https://doi.org/https://doi.org/10.1002/asl.316

Kravitz, B., et al. (2021). Identifying the sources of uncertainty in climate model simulations of solar radiation modification with the g6sulfur and g6solar geoengineering model intercomparison project (geoMIP) simulations. *Atmos. Chem. Phys., 21, p. 10039-10063*. https://doi.org/https://doi.org/10.5194/acp-21-10039-2021

Lohmann, U., et al. (1993). The köppen climate classification as a diagnostic tool for general circulation models. *Climate Research, 3(3), p. 177-193*. https://doi.org/https://www.jstor.org/stable/24863394

MacMartin, D., & Kravitz, B. (2019). Mission-driven research for stratospheric aerosol geoengineering. *Perspective, Vol. 116, No. 4*. https://doi.org/https://doi.org/10.1073/pnas.1811022116

NOAA. (n.d.). *Waht is the atlantic meridional overturning circulation (AMOC)?* https://oceanservice.noaa.gov/facts/eutrophication.html

Pamplany, A., et al. (2020). The ethics of geoengineering: A literature review. *Science and Engineering Ethics 26, 3069-3119*. https://doi.org/https://doi.org/10.1007/s11948-020-00258-6

Peel, M., et al. (2007). Updated world map of the köppen-geiger climate classification. *Hydrol. Earth Syst. Sci., 11, 1633-1644*. https://doi.org/https://doi.org/10.5194/hess-11-1633-2007

Robock, A., et al. (2009). Benefits, risks, and costs of stratospheric geoengineering. *Geophysical Research Letters, Vol 36, Issue 19*. https://doi.org/https://doi.org/10.1029/2009GL039209

Self, S., et al. (1993). The atmospheric impact of the 1991 mount pinatubo eruption. https://doi.org/https://ntrs.nasa.gov/api/citations/19990021520/downloads/19990021520.pdf

Smith, W., & Wagner, G. (2018). Stratospheric aerosol injection tactics and costs in the first 15 years of deployment. *Environmental Research Letters, Vol 13, Number 12*. https://doi.org/https://doi.org/10.1088/1748-9326/aae98d

Tilmes, S., et al. (2018). CESM1 (WACCM) stratospheric aerosol geoengineering large ensemble project. *American Meteorological Society, p. 2361–2371*. https://doi.org/https://doi.org/10.1175/BAMS-D-17-0267.1

Tilmes, S., et al. (2020). Reaching 1.5 and 2.0 ºC global surface temperature targets using stratospheric aerosol geoengineering. *Earth Syst. Dynam., 11, p. 579-601*. https://doi.org/https://doi.org/10.5194/esd-11-579-2020

Tracy, S., et al. (2022). Stratospheric aerosol injection may impact global systemx and human health outcomes. *Elementa: Science of the Anthropocene*. https://doi.org/https://doi.org/10.1525/elementa.2022.00047

Xie, M., et al. (2022). Impacts of three types of solar geoengineering on the atlantic meridional overturning circulation. *European Geosciences Union, Vol 22 Issue 7, p. 4581-4597*. https://doi.org/https://doi.org/10.5194/acp-22-4581-2022

Zarnetske, P., et al. (2021). Potential ecological impacts of climate intervention by reflecting sunlight to cool earth. *Perspective, Vol. 118, No. 15*. https://doi.org/https://doi.org/10.1073/pnas.1921854118

6 Appendices

6.1 Appendix 1

This appendix shows the climatology plots for all the regions. These plots show the monthly mean over the last 15 years for every simulation: grey for REF, blue for CONTROL, orange for SAI 2020 and green for SAI 2080. The bars show the total precipitation (left axis) and the lines the reference height temperature (right axis).

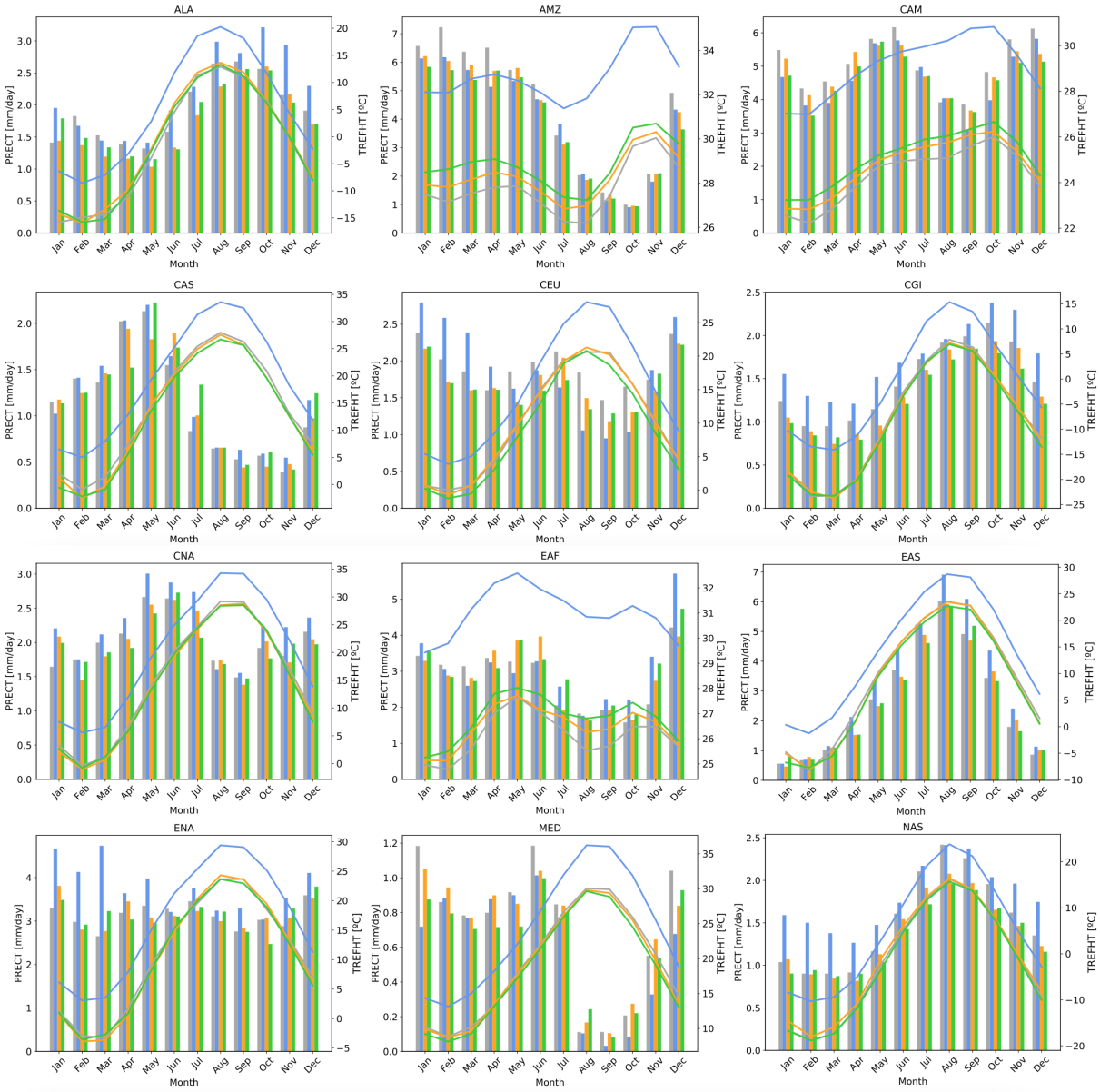

Figure 20: Climatology plots for 12 regions. The bars show the total precipitation (left axis) and the lines the reference height temperature (right axis). Blue is for the CONTROL simulation, orange for SAI 2020, green for SAI 2080 and grey for REF.

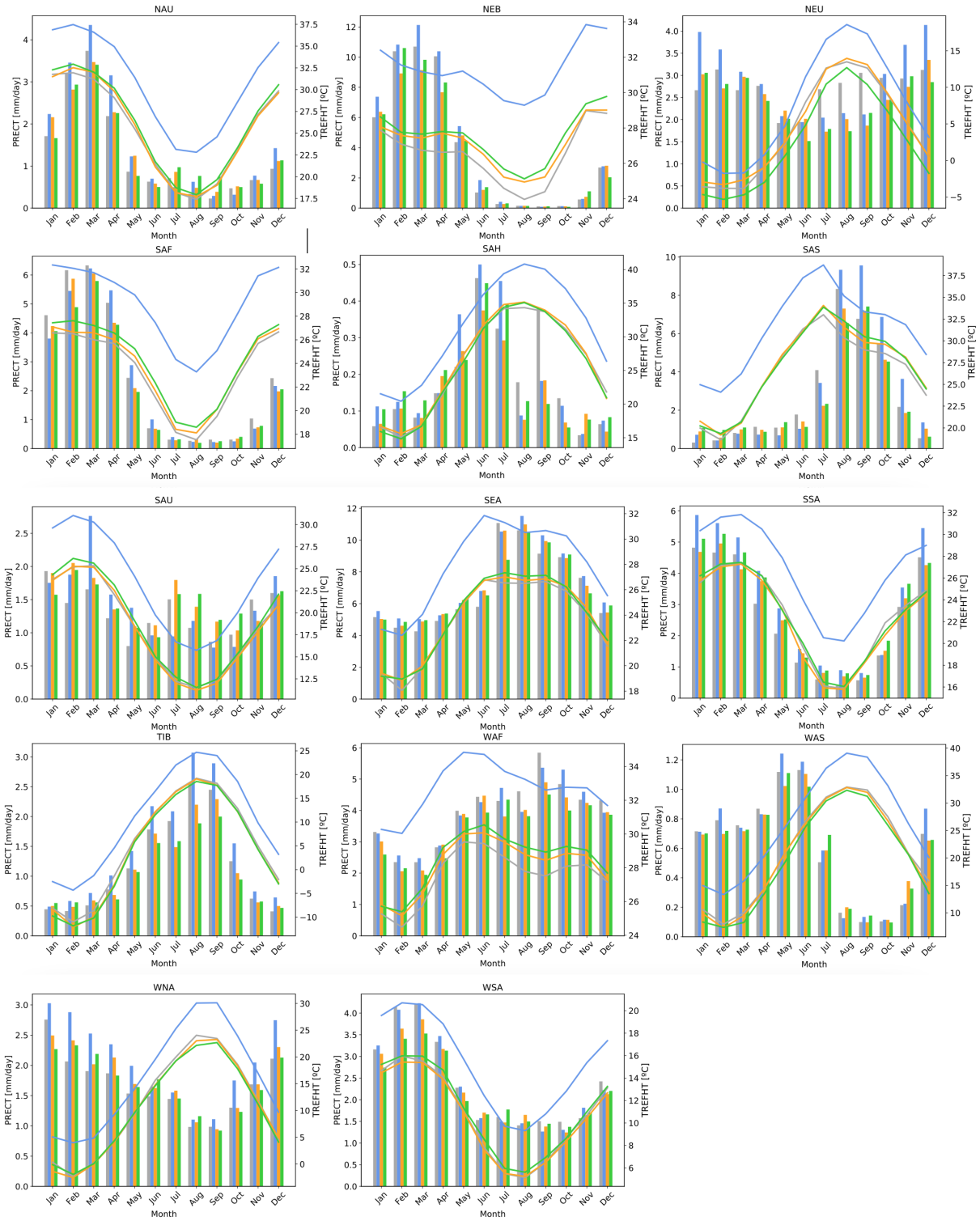

Figure 21: Climatology plots for the other 14 regions. The bars show the total precipitation (left axis) and the lines the reference height temperature (right axis). Blue is for the CONTROL simulation, orange for SAI 2020, green for SAI 2080 and grey for REF.

6.2 Appendix 2

This appendix shows the seasonal exacerbation plots for the reference height temperature, the total precipitation and the precipitation minus evaporation.

Both figures from this appendix resemble Figure 10, except that in this case the points seem to be more spread out, specially in the plots for the third column. Still looking at the last column, in Figure 22 we can clearly see a few points that overcool in SAI 2080 in comparison to SAI 2020. As explained in Section 4.3, they correspond to the grid cells near the AMOC.

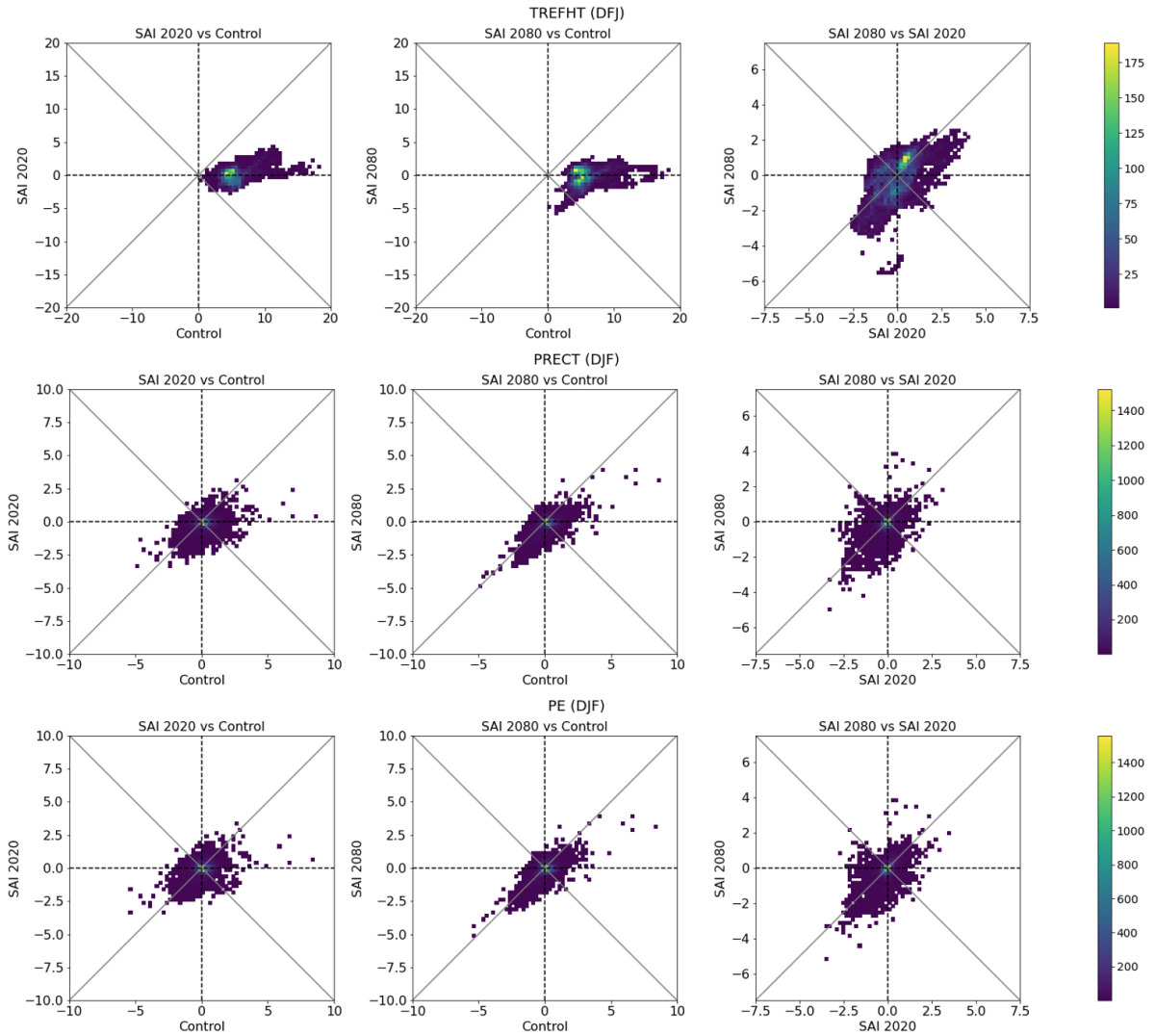

Figure 22: 2085-2100 average exacerbation plots with respect to the reference period for the months of December, January and February. From top to down, they show TREFHT, PRECT and PE. Every point represents a grid cell.

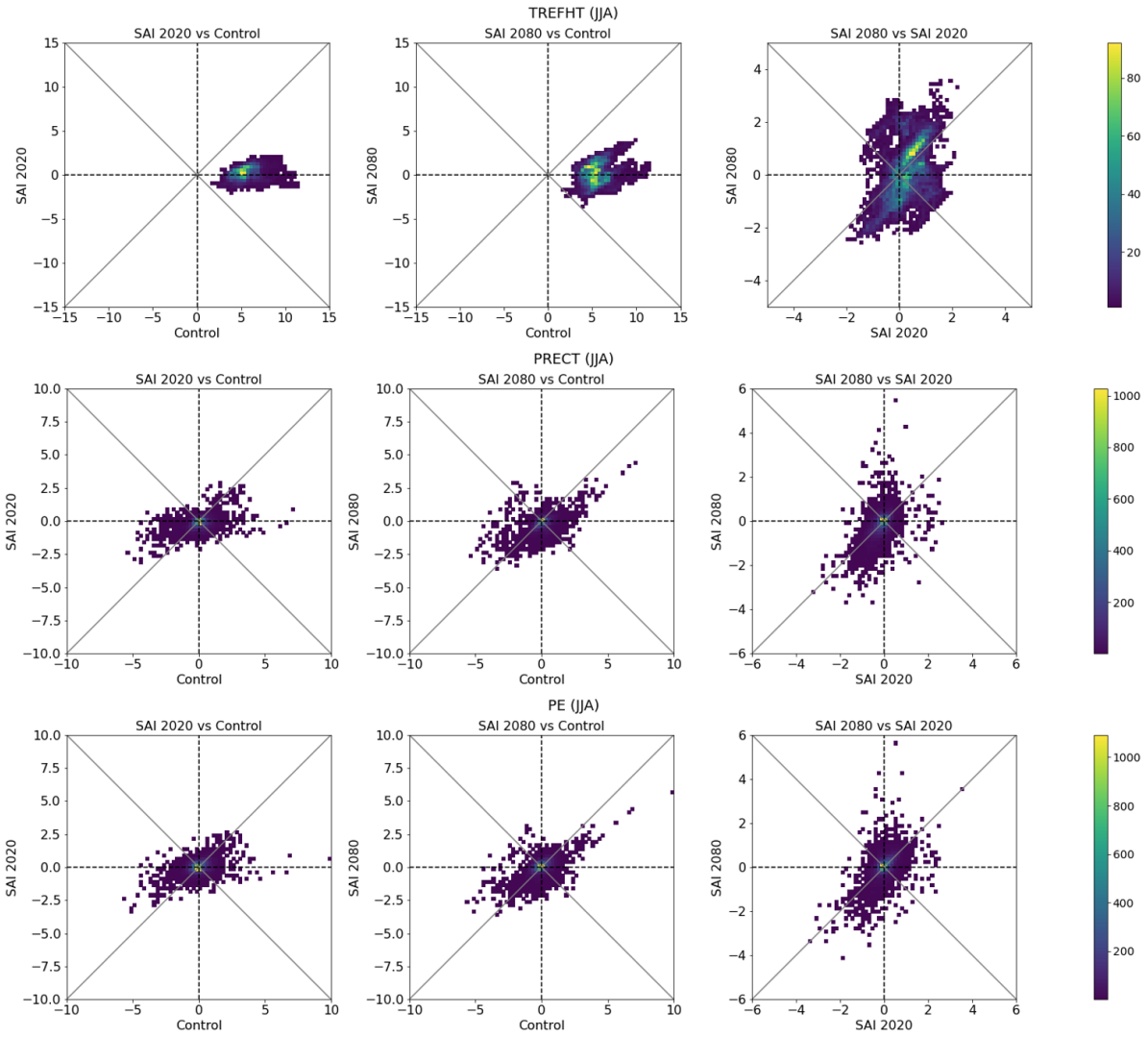

Figure 23: 2085-2100 average exacerbation plots with respect to the reference period for the months of June, July and August. From top to down, they show TREFHT, PRECT and PE. Every point represents a grid cell.

6.3 Appendix 3

This appendix shows the Köppen climate diagrams for SAI 2080 and the CONTROL average between 2060 and 2080. This comparison is made to better visualize the effectiveness of SAI 2080.

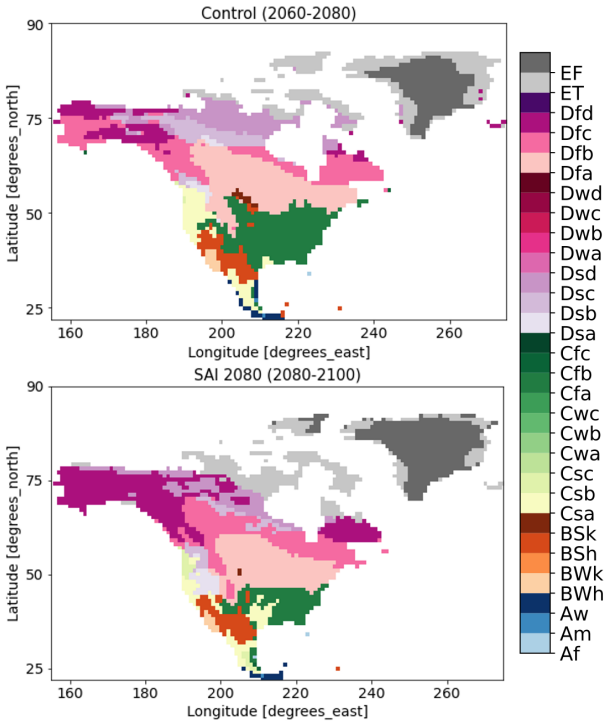

Figure 24: Köppen climate classification for Canada and Greenland. The upper plot shows CONTROL from 2060 to 2080, and the bottom one SAI 2080 for 2080 until 2100. The color legend indicates the groups presented in Section 2.3.2.

As explained in Section 3.2.1, SAI 2080 is able to bring the climate close to how it was during the reference period, which indicates that SAI 2080 is able to partially restore the climate.